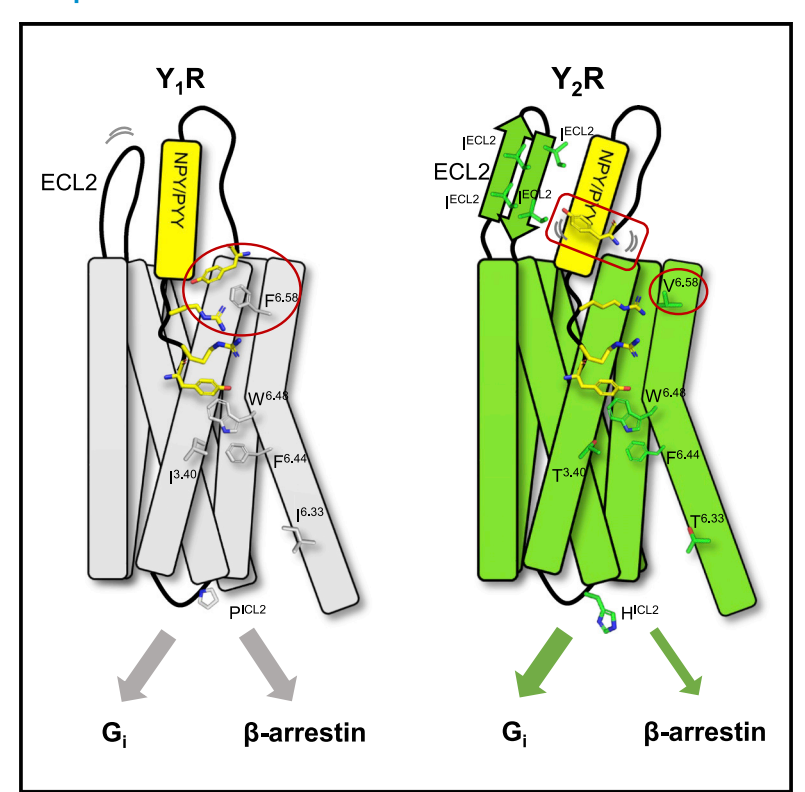
Structural basis for Y2 receptor-mediated neuropeptide Y and peptide YY signaling

Graphical abstract



Authors

Hyunook Kang, Chaehee Park, Yeol Kyo Choi, ..., Chaok Seok, Wonpil Im, Hee-Jung Choi

Correspondence

choihj@snu.ac.kr

In brief

Kang et al. determined the cryo-EM structures of Y_2R bound to its endogenous ligands NPY and PYY(3–36), which explains the tolerance of Y_2R to N-terminal truncation of the peptide ligand. Structural comparison of NPY– Y_2R with NPY– Y_1R revealed distinct binding modes of NPY to Y_1R and Y_2R .

Highlights

- Cryo-EM structures of active Y₂R bound to its endogenous ligands, NPY and PYY(3–36)
- N-terminal region of NPY/PYY(3–36) does not make a direct contact with Y₂R
- Residue at position 6.58 is important for receptor subtypespecific NPY binding
- Y₁R and Y₂R display different downstream regulator selectivities









Article

Structural basis for Y2 receptor-mediated neuropeptide Y and peptide YY signaling

Hyunook Kang,^{1,4} Chaehee Park,^{1,4} Yeol Kyo Choi,² Jungnam Bae,¹ Sohee Kwon,³ Jinuk Kim,¹ Chulwon Choi,¹ Chaok Seok,3 Wonpil Im,2 and Hee-Jung Choi1,5,*

- ¹Department of Biological Sciences, Seoul National University, Seoul 08826, Republic of Korea
- ²Department of Biological Sciences, Lehigh University, Bethlehem, PA 18015, USA
- ³Department of Chemistry, Seoul National University, Seoul 08826, Republic of Korea
- ⁴These authors contributed equally
- 5Lead contact

*Correspondence: choihj@snu.ac.kr https://doi.org/10.1016/j.str.2022.11.010

SUMMARY

Neuropeptide Y (NPY) and its receptors are expressed in various human tissues including the brain where they regulate appetite and emotion. Upon NPY stimulation, the neuropeptide Y1 and Y2 receptors (Y1R and Y₂R, respectively) activate G₁ signaling, but their physiological responses to food intake are different. In addition, deletion of the two N-terminal amino acids of peptide YY (PYY(3-36)), the endogenous form found in circulation, can stimulate Y₂R but not Y₁R, suggesting that Y₁R and Y₂R may have distinct ligand-binding modes. Here, we report the cryo-electron microscopy structures of the PYY(3-36)-Y₂R-G_i and NPY-Y₂R-G_i complexes. Using cell-based assays, molecular dynamics simulations, and structural analysis, we revealed the molecular basis of the exclusive binding of PYY(3-36) to Y_2R . Furthermore, we demonstrated that Y_2R favors G protein signaling over β -arrestin signaling upon activation, whereas Y_1R does not show a preference between these two pathways.

INTRODUCTION

Neuropeptide Y (NPY) is one of the most abundant neuropeptides in the brain and is known to activate the neuropeptide Y receptor (NPYR) family. In human, the NPYR family, which belongs to class A G protein-coupled receptors (GPCRs), includes four subtypes-Y₁R, Y₂R, Y₄R, and Y₅R-that are expressed differently throughout the body, including the brain. NPYR activation is involved in diverse physiological processes, such as food intake, fear, anxiety, memory retention, and bone formation.²⁻⁵ Therefore, these receptors are considered a therapeutic target for related diseases, such as obesity, anxiety disorder, memory loss, osteoporosis, and cancer. 1,6-9

In addition to NPY, two other homologous neuropeptides, peptide YY (PYY) and pancreatic polypeptide (PP), also bind to NPYR with specificity. In contrast to NPY, which is mainly expressed in neuronal regions, PYY and PP are mainly expressed in the gastrointestinal tract¹⁰ and play a role in regulating food intake and energy expenditure. 11,12 These three peptides share high sequence homology but display different preferences toward NPYR subtypes. Whereas NPY and PYY have high potency toward Y1R, Y2R, and Y5R, PP shows high potency only toward Y₄R. 13

Although both Y₁R and Y₂R can be activated by NPY/PYY with similar potency, they display different reactivity toward the N-terminally truncated form of NPY/PYY. 14,15 A deleted form of PYY missing the two N-terminal amino acids, PYY(3-36), is an endogenous form found in circulation after cleavage of PYY released from the gastrointestinal tract upon food intake; PYY(3-36) preferentially activates Y₂R but not Y₁R. ^{15,16} In addition, upon NPY/PYY activation, Y₁R and Y₂R exhibit different physiological responses in some cases. Regarding appetite regulation, NPY-induced Y₁R enhances food intake, whereas NPY-induced Y₂R suppresses appetite.¹⁷ Thus, efforts have been made to develop a PYY(3-36) analog that selectively activates Y2R rather than Y1R and utilize it as a drug for treating obesity. In fact, a PYY analog agonist is under development as a weight loss drug. 18 In addition, it has been reported that NPYRs are overexpressed in several types of cancer. Elevated Y1R expression has been reported in primary breast cancer. In neuroblastoma tissues, Y₂R expression was shown to be particularly increased, which mediates the stimulation of tumor cell proliferation and angiogenesis. 19 Thus, some studies have used Y2R-selective antagonists to slow down neuroblastoma progression and Y2R-selective NPY analog agonists as a carrier for boron neutron capture therapy. 19,20

Recent structural studies of the NPY-Y₁R-G_i complex have elucidated the molecular mechanism of NPY recognition by Y₁R, ^{21,22} which explains why Y₁R requires the complete N terminus of NPY for its optimal activation. However, the molecular basis for Y2R activation by PYY(3-36) and the differences in



Article



downstream signaling of NPY/PYY through Y_1R and Y_2R have not been fully revealed.

In this study, we present two cryo-electron microscopy (cryo-EM) structures of the active state-Y₂R bound to its endogenous ligands, NPY and PYY(3-36), at 3.11- and 2.95-Å resolution, respectively. Based on structural analysis and comparison of these two structures with that of the NPY-Y1R complex, we identify conserved and distinct NPY binding modes to Y₁R and Y₂R. Using molecular dynamics (MD) simulations and functional analysis, we provide an important structural insight into Y₂R activation and the molecular mechanism of exclusive binding of PYY(3-36) to Y₂R. In addition, using bioluminescence resonance energy transfer (BRET) assays, we investigated the difference in the coupling efficiencies of Y₁R and Y₂R for downstream transducers, G_i and β-arrestin 2. Our results show that Y₂R has lower coupling efficiency for β-arrestin 2 than Y₁R, which can be increased by mutating some residues from the transmembrane domain (TMD) and the intracellular loop 2 (ICL2).

RESULTS

Overall structure of NPY/PYY(3-36)-bound Y₂R

In our previous study, the N-terminally truncated peptides NPY(3-36) and PYY(3-36) were shown to elicit a 12- to 18-fold reduction of Y₁R-mediated G_i signaling.²¹ For comparison, in this study, we performed calcium signaling assays following an identical experimental protocol and using Y2R. Our results showed that NPY(3-36) and PYY(3-36) have wild-type ligandlike potency at Y₂R (a 1.5- to 2.3-fold increase in half-maximum effective concentration (EC₅₀) value) (Figure S1 and Table S1). This is in line with a previous study reporting that NPY(2-36) or PYY(3-36) show wild-type affinity toward Y₂R, but 83- or 690-fold increased half-maximum inhibitory concentration (IC₅₀), respectively, toward Y₁R.²³ Using isothermal calorimetry (ITC), we also showed that NPY, PYY, and NPY(18-36) display similar binding affinities toward Y₂R with K_D values in the range of 2.7-4 μM in the absence of G_i protein (Figure S1), suggesting that the NPY N terminus is not essential for Y2R binding, at least in in vitro systems.

To understand the molecular basis of the exclusive binding of PYY(3–36) to Y₂R and compare the binding modes of NPY to Y₁R and Y₂R, we determined the cryo-EM structures of the PYY(3-36)-Y₂R-G_i-scFv16 and NPY-Y₂R-G_i-scFv16 complexes. Initially, we attempted to purify wild-type Y₂R for this structural study; however, this was unsuccessful because of the low expression level. Introduction of two mutations, H1493.51Y and S280^{6.47}C (superscripts indicate Ballesteros-Weinstein numbering²⁴), which was used to determine the crystal structure of the antagonist-bound Y₂R,²⁵ significantly enhanced the expression level of Y2R in baculovirus-mediated expression in insect cells. We confirmed that the H149^{3.51}Y/S280^{6.47}C mutation did not affect G_i signaling upon NPY/PYY(3-36) binding using calcium signaling assays (Figure S2). Using this mutant Y₂R, we successfully purified the PYY(3-36)-Y₂R-G_i-scFv16 and NPY-Y2R-Gi-scFv16 complexes and determined their cryo-EM structures at a nominal resolution of 2.95 and 3.11 Å, respectively (Figures 1A and S3 and Table 1). The cryo-EM density for each peptide ligand, which protrudes into the extracellular region, allowed us to identify residues 17-36 of each peptide

Table 1. Cryo-EM data collection and structure refinement statistics

statistics		
	PDB: 7YON, EMD-33984 PYY(3-36)- Y_2R-G_i -scFv16	PDB: 7YOO, EMD-33985 NPY-Y ₂ R- G _i -scFv16
Data collection and processi	ng	
Magnification (nominal)	1,050,000	1,050,000
Voltage (kV)	300	300
Electron exposure (e ⁻ /Å ²)	60.5	66
Defocus range (μm)	$-0.75 \sim -2.0$	$-1 \sim -2.25$
Pixel size (Å)	0.849	0.8415
Symmetry imposed	C1	C1
Initial particle images (no.)	12,262,301	9,842,630
Final particle images (no.)	359,459	500,366
Map resolution (Å)	3.15 (TMD) 2.95 (global)	3.39 (TMD) 3.11 (global)
FSC threshold	0.143	0.143
Map sharpening B factor (Å ²)	-116.2 (TMD) -102.6 (global)	-116.8 (TMD) -118.1 (global)
Refinement		
Initial model used (PDB code)	7DDZ, 7VGX	7DDZ, 7VGX
Model composition		
Non-hydrogen atoms	9,163	9,188
Protein residues	1,165	1,168
Ligands	TYC: 1	TYC: 1
Water	2	
B factors (Ų)		
Protein	41.11	57.89
Ligand	36.53	60.15
RMS deviations		
Bond lengths (Å)	0.003	0.002
Bond angles ()	0.483	0.431
Validation		
MolProbity score	1.29	1.16
Clashscore	3.66	3.71
Rotamer outliers (%)	0.00	0.00
CaBLAM outliers (%)	1.69	1.68
EMRinger score	3.97	3.56
Ramachandran plot		
Favored (%)	97.29	98.26
Allowed (%)	2.71	1.74
Outliers (%)	0.00	0.00

(Figure S3). In contrast, the remaining N-terminal residues of the peptides were not well resolved because of weak density; therefore, only the N-terminal residues 3–7 of PYY(3–36) and 1–8 of NPY are included in each final model (PDB: 7YON and 7YOO, respectively). The overall structures of Y_2 R in the two complexes are almost identical and exhibit conserved features of the G_i -bound active state of class A GPCRs, such as conformational changes at the C(/S)WxP, PI(/T)F, DRY(/H), and NPxxY motifs upon activation (Figure S4). Previously, a rotamer



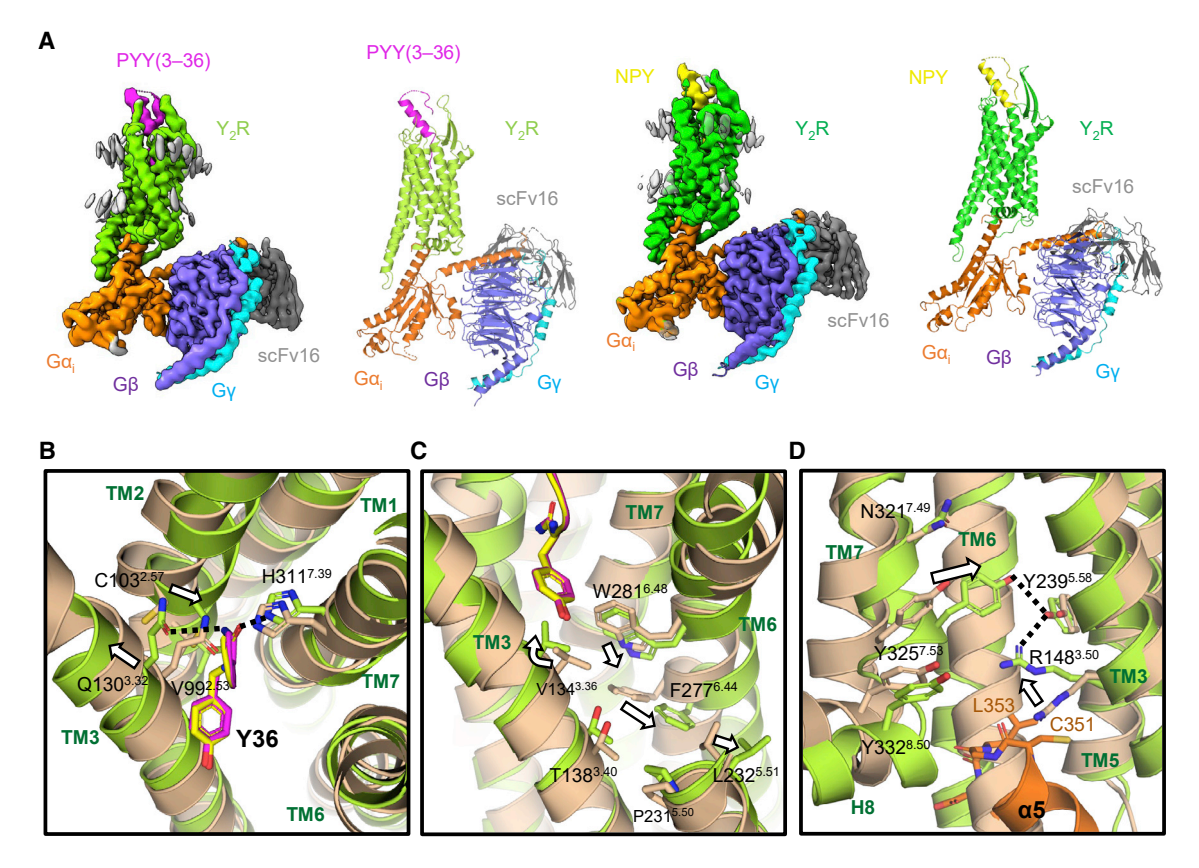


Figure 1. Overall structures of NPY/PYY(3-36)-Y2R-G1-scFv16 complexes and structural comparison between inactive and active Y2R (A) Cryo-EM maps and overall structures of PYY(3-36)-Y2R-Gi-scFv16 (left) and NPY-Y2R-Gi-scFv16 (right). Cryo-EM maps and structure models of PYY(3-36), Y₂R bound to PYY(3–36), NPY, Y₂R bound to NPY, Gα₁, Gβ, Gγ, and scFv16 are colored in magenta, lime, yellow, green, orange, purple-blue, cyan, and dark gray, respectively. See also Figure S3.

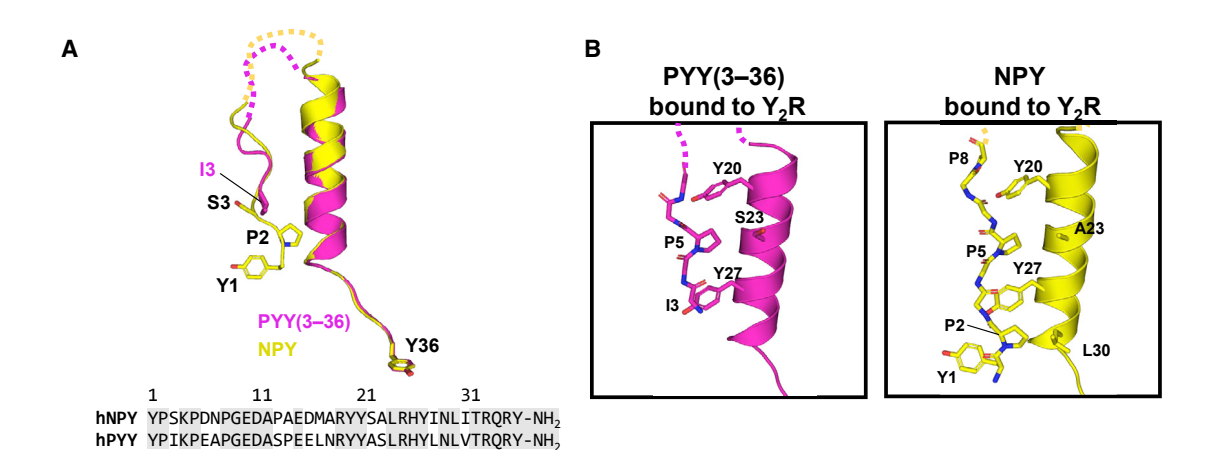
(B) Superposition of inactive Y₂R bound to antagonist, JNJ-31020028 (colored in light brown; PDB: 7DDZ) and active Y₂R (only PYY(3-36)-bound Y₂R is shown as a representative). The polar interaction between Q130^{3,32} and H311^{7,39} is disrupted by NPY/PYY(3–36) interaction. Q130^{3,32} moves upward for the interaction with the C-terminal amide group of NPY/PYY(3-36), and C103^{2.57} stabilizes this interaction by making van der Waals contacts with both. See also Figure S4. (C) Conformational changes in the C(/S)WxP and PI(/T)F motifs. Ligand binding induces a rotamer change of V134^{3,36} and downward shift of W281^{6,48}, which pushes F277^{6.44} outward. See also Figure S4.

(D) Conformational changes in the NPxxY and DRY(/H) motifs. The inward movement of Y325 $^{7.53}$ breaks the π - π interaction with Y332 $^{8.50}$ and polar interaction with N321^{7,49}, but instead it forms a new interaction network with R148^{3,50} and Y239^{5,58}. Upon Ga, binding, the rotamer of R148^{3,50} changes upward (indicated by the white arrow) to avoid steric collision with the $\alpha 5$ helix of $G\alpha_i$. See also Figure S4.

change of Gln at position 3.32 was proposed to be a key event in a series of conformational changes during activation of Y1R and orexin receptor type 2.21,27 Similarly, upon peptide ligand binding to Y₂R, the polar interaction between Q130^{3.32} and H311^{7,39} was disrupted by Y36, and the two residues formed hydrogen bonds with the C-terminal amide group of Y36 (Figure 1B). With the Q130^{3.32} upward shift, V99^{2.53} and C103^{2.57} of TM2 moved inward by 2-2.5 Å, forming an extensive hydrophobic interaction network with A133^{3,35}, V134^{3,36}, W281^{6,48}, A314^{7.42}, and M315^{7.43}, which comprise the base of the ligandbinding pocket. Peptide ligand-induced conformational changes include a rotamer change of L232^{5.51}, which is associated with a conformational change of F277^{6.44} in the PI(/T)F motif (Figure 1C) and an outward movement of the cytoplasmic part of TM6 by 11.5-11.9 Å (Figure S4). To avoid the steric collision with the $\alpha 5$ helix of $G\alpha_{\text{i}},$ an upward rotamer change of R148 $^{3.50}$ was observed upon $G\alpha_i$ binding, which disrupts the interaction with T85^{2.39}, T266^{6.33}, and T267^{6.34} and forms polar and van der Waals contacts with the carbonyl of C351 and L353 of the α 5 helix of $G\alpha_i$, respectively (Figure S4). In addition, upon activation, in association with an inward movement of TM7 by 4.1-4.4 Å, Y325^{7.53} in the NPxxY motif, a highly conserved residue, undergoes a large conformational shift by breaking the π - π interaction with Y3328.50 and forming a new interaction network with R148^{3.50} in the DRY(/H) motif and Y239^{5.58} (Figures 1D and S4).

At the extracellular part of the TMD, a relatively small but noticeable movement of TM helices was observed. Upon ligand binding, the extracellular tips of TM4 moved outward by \sim 1.6 Å, and the C-terminal ends of TM2 moved inward by ~2 Å (Figure S4). TM movement is associated with conformational changes of extracellular loops (ECLs). In particular, ECL2, which forms β-strands, moved outward by 1.7-2.5 Å upon ligand binding. The details of the molecular interactions of peptide ligands with Y2R are described in the next section.





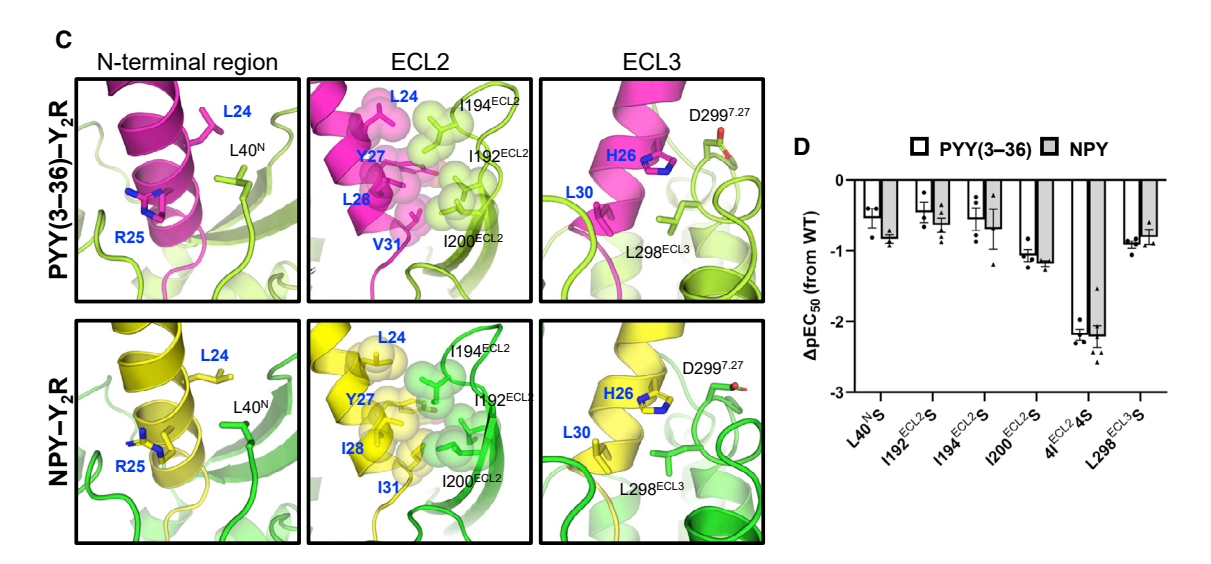


Figure 2. NPY/PYY(3-36) binding at the extracellular region of Y₂R

(A) Structural alignment of NPY and PYY(3-36) bound to Y₂R (top). Missing residues are represented as dotted lines. Sequence alignment of human NPY and PYY (bottom). Conserved residues between NPY and PYY are colored in gray.

(B) Both NPY and PYY(3-36) establish an intramolecular hydrophobic network between the N-terminal loop and helical region, stabilizing a PP-fold. (C) The N-terminal region, ECL2, and ECL3 of Y₂R participate in NPY and PYY(3-36) binding. The color codes of NPY, PYY(3-36), and Y₂R follow those in Figure 1. $NPY/PYY(3-36) \ residues \ are \ labeled \ in \ blue. \ (Left) \ L40^N \ at \ the \ N-terminal \ region \ is \ in \ close \ contact \ with \ L24 \ and \ R25. \ (Middle) \ l192^{ECL2}, \ l194^{ECL2}, \ l195^{ECL2}, \ l195^{ECL2},$ F198^{ECL2}, and I200^{ECL2} form hydrophobic contacts with L24, Y27, L28, and V31 of PYY(3-36) or L24, Y27, I28, and I31 of NPY. Although L28/I28 and V31/I31 are not conserved between two peptides, van der Waals contacts (represented as transparent spheres) are similarly formed in the two structures. (Right) L298 ECL3 and D299^{7.27} form van der Waals contacts with H26 and L30.

(D) Differences in pEC₅₀ for each Ser mutant of key hydrophobic residues of Y₂R relative to wild-type Y₂R. Δ pEC₅₀ values for the treatment of PYY(3–36) and NPY are shown in white and gray bar graphs, respectively. Bar graphs and error bars indicate means and SEMs obtained from independent experiments of Ca²⁺ signaling assays (represented as symbols), respectively. See also Figure S2.

NPY/PYY binding mode in Y₂R

Structural analysis of the NPY and PYY(3-36) when bound to Y₂R shows that both structures align well with a root-mean-square deviation (RMSD) of 1 Å for 25 Cα atoms (Figure 2A). In both structures, the N-terminal region of the peptide does not establish any notable interactions with Y2R. Instead, intramolecular van der Waals contacts of P2-D6 and P8 of NPY or I3-P5 and A7 of PYY(3-36) with Y20, A23/S23, and Y27 in the helical region of NPY/PYY(3-36) are observed (Figure 2B). This conformation, termed the PP-fold, was previously reported as an important structural feature stabilizing the structures of PYY (PDB: 2DEZ) and PP (PDB: 1BBA), 28-30 but the PP-fold was not observed in the solution structure of NPY. 31,32 The recently published structure of NPY-Y₁R, however, shows that NPY forms a PP-fold when bound to Y₁R.^{21,22} In our structure, the stability of the PP-fold of NPY complexed with Y2R was also investigated by MD simulations. In one of three independent 1-µs simulations, the N terminus of NPY dissociated from the helical region of NPY, whereas in the other two replicates, the intramolecular interaction appeared to be maintained, as indicated by the constant distance between the $C\alpha$ atoms of P5 and Y20 (Figure S5). However, the distance between $C\alpha$ atoms of Y1 and G216^{5.35} was observed to be varied in three replicates, suggesting that Y1 occupies different space in each replicate (Figure S5). Thus,





while the PP-fold of peptide is maintained by intramolecular interaction between the NPY N-terminal region and the NPY helix, NPY N terminus (Y1) is subjected to dynamic motion and is not directly involved in intramolecular and Y₂R-specific interactions. NPY and PYY have overall 67% sequence identity, but among residues 3-7 of PYY observed in the PYY(3-36)-bound Y₂R structure, only K4 and P5 are conserved in NPY (Figure 2A). Despite the weak density at the N-terminal region, it is clear that K4 and P5 of PYY are well aligned with the corresponding residues of NPY, participating in intramolecular interactions and maintaining the PP-fold. This suggests that the PP-fold is favored by the NPY family when bound to receptor, regardless of the peptide type and the absence of the two N-terminal amino

Our cryo-EM map showed a clear density for peptide residues 17-36, forming a helical structure (residues 17-31) and an extended conformation (residues 32-36) (Figure S3). The helical region protrudes from the TMD and is surrounded by three parts of the receptor: the N-terminal region, ECL2, and ECL3 (Figure 2C). We could not model all the residues of the N-terminal region of Y₂R, but cryo-EM density clearly showed that L40^N is in close contact with L24 and R25 of NPY/PYY(3-36). The importance of L40^N in NPY/PYY(3-36) signaling was demonstrated by the 3.7- to 4.5-fold reduction in the signaling of L40^NS Y₂R (Figures 2D and S2 and Table S1).

One of the interesting features by which Y2R recognizes NPY/ PYY(3-36) is the hydrophobic interactions through ECL2, which contains an Ile-rich region. A previous mutagenesis study has identified I192 ECL2, I194 ECL2, and I200 ECL2 as important residues for NPY recognition. 33 Our structures show that these Ile residues form hydrophobic interactions with L24, Y27, I28/L28, and I31/V31 of NPY/PYY, although V31 of PYY has fewer contacts than I31 of NPY (Figure 2C). The I192^{ECL2}S and I194^{ECL2}S mutations resulted in a 2.8- to 4.4-fold decrease in NPY/PYY(3-36) signaling, whereas the I200^{ECL2}S mutation displayed more than 10-fold reduced signaling (Table S1). Indeed, I200^{ECL2} is located at the core of the hydrophobic network between Y2R and peptide ligand. The introduction of four Ile mutations in ECL2 (4IECL2S)-I192ECL2S, I194^{ECL2}S, I195^{ECL2}S, and I200^{ECL2}S—resulted in a synergistic effect showing 160-fold decrease in NPY/PYY(3-36) signaling (Figures 2D and S2 and Table S1). To investigate the dynamics of the NPY helix interaction, MD simulations were performed. Three independent 1- μ s MD simulations revealed that the α -helix of NPY bound to Y₂R showed fewer motions than that of NPY bound to Y₁R. In the simulations, the tilted angle of the NPY helical axis was maintained within the range of 28°-58° (Figure S5), whereas in the case of NPY-bound Y1R, the NPY helical axis varied in the range of 5° – 70° .²¹ Additionally, the minimum distance between all atoms of the α-helix and ECL2 was nearly constant and within \sim 1 Å variation in all replicates (Figure S5), suggesting that the interaction between the NPY helix and ECL2 of Y2R was maintained in the simulations. Compared with ECL2, ECL3 establishes relatively fewer contacts with NPY/PYY(3-36). L298^{ECL3} forms van der Waals contacts with H26 and L30 of NPY/PYY(3-36) (Figure 2C), and its contribution to downstream signaling was demonstrated by reduced NPY/PYY(3-36) signaling of the L298^{ECL3}S mutation (Figures 2D and S2 and Table S1).

Residues 32-36 comprising the C-terminal tail are identical between the two peptides. The five C-terminal amino acids are

located inside the TMD, engaging Y2R through extensive polar and hydrophobic interactions. The phenyl group of Y36 is located at the base of the hydrophobic ligand-binding pocket, and the hydroxyl group forms polar contacts with S223^{5,42} (Figure 3A). Our signaling assays using Y36F and Y36A NPY mutants showed a 5.8-fold and 85-fold increase, respectively, in EC₅₀ values toward Y2R (Figure S2 and Table S1), suggesting a greater contribution of the hydrophobic phenyl group than the hydroxyl group of Y36 to Y2R binding. The amidated C terminus forms polar interactions with T107^{2.61}, Q130^{3.32}, and H311^{7.39} (Figure 3A), which are conserved in all NPY receptor subtypes, implying the conserved interaction pattern between amidated peptides and NPYRs. The importance of these residues was demonstrated by mutagenesis study (Figure 3B and Table S1).

With Y36 as the bottom center, T32/Q34 and R33/R35 extend toward TM2 and TM5/6, respectively, R33 and R35 form extensive polar contacts with E205^{45.52}, S220^{5.39}, Q288^{6.55}, and D292^{6.59} (Figure 3C). Of these residues, D292^{6.59}, which is highly conserved in the NPY receptor family, appears to be essential for receptor binding, as the D292^{6.59}A mutant showed the most dramatic decrease in NPY/PYY(3-36) signaling with a 200- and 220-fold increase in EC₅₀ values (Figures 3B and S2 and Table S1). Indeed, D292^{6.59} directly forms a salt bridge with R33 and indirectly participates in the polar interaction with R35 through S220^{5.39} (Figure 3C). T32 and Q34 form van der Waals contacts with T107^{2.61}. Y110^{2.64}, T111^{2.65}, and F307^{7.35} (Figure 3D). In our PYY(3-36)bound Y2R structure, we identified two water molecules (W1 and W2) in the ligand binding pocket with a local resolution of 2.5-2.8 Å (Figure S3). W1 forms hydrogen bonds with Y36 and R35 of PYY as well as with S223^{5.42}, and W2 mediates the interaction of Q34 of PYY with Q130^{3.32} (Figures 3C and 3D). A previous study showed that mutant PYY Q34P had a K_i value of 710 nM against 100 pM of 125I-PYY, whereas PYY(3-36) has a Ki value of 0.11 nM,34 which may be explained by the loss of polar contacts with T107^{2.61} and T111^{2.65} and water-mediated interaction with Q130^{3.32} as shown in this structure.

Overall, NPY and PYY(3-36) have similar binding modes to Y₂R, with the N-terminal region having a relatively low sequence identity and not being involved in receptor binding.

Receptor subtype-specific interactions of NPY

Using the recently published NPY-bound Y₁R structure,²¹ we analyzed the conserved and receptor subtype-specific interactions of NPY with Y₁R and Y₂R. Surprisingly, when the receptors from the two complexes were aligned, the corresponding NPY structures did not align well (RMSD for 22 Cα atoms of 4.1 Å). Whereas the positions of R35 and Y36 were aligned well in both complex structures, the remaining amino acids of NPY occupied different positions. Overall, the NPY helix bound to Y₂R rotated 39° clockwise, and the angle of the helix axis of NPY to the membrane was tilted by 6° compared with that in the NPY-Y₁R complex (Figure 4A). Furthermore, the N termini of NPY in the two structures occupied completely different positions. This is a fairly unique case, distinct from the cases reported so far in that the ligand-binding modes to receptor subtypes within the same GPCR family are mostly similar. To date, the structures of eight pairs of class A GPCR subtypes bound to the same ligand have been reported; these include $\beta1$ - and $\beta2$ adrenergic receptors (β_1AR and β_2AR) bound to epinephrine^{35,36}



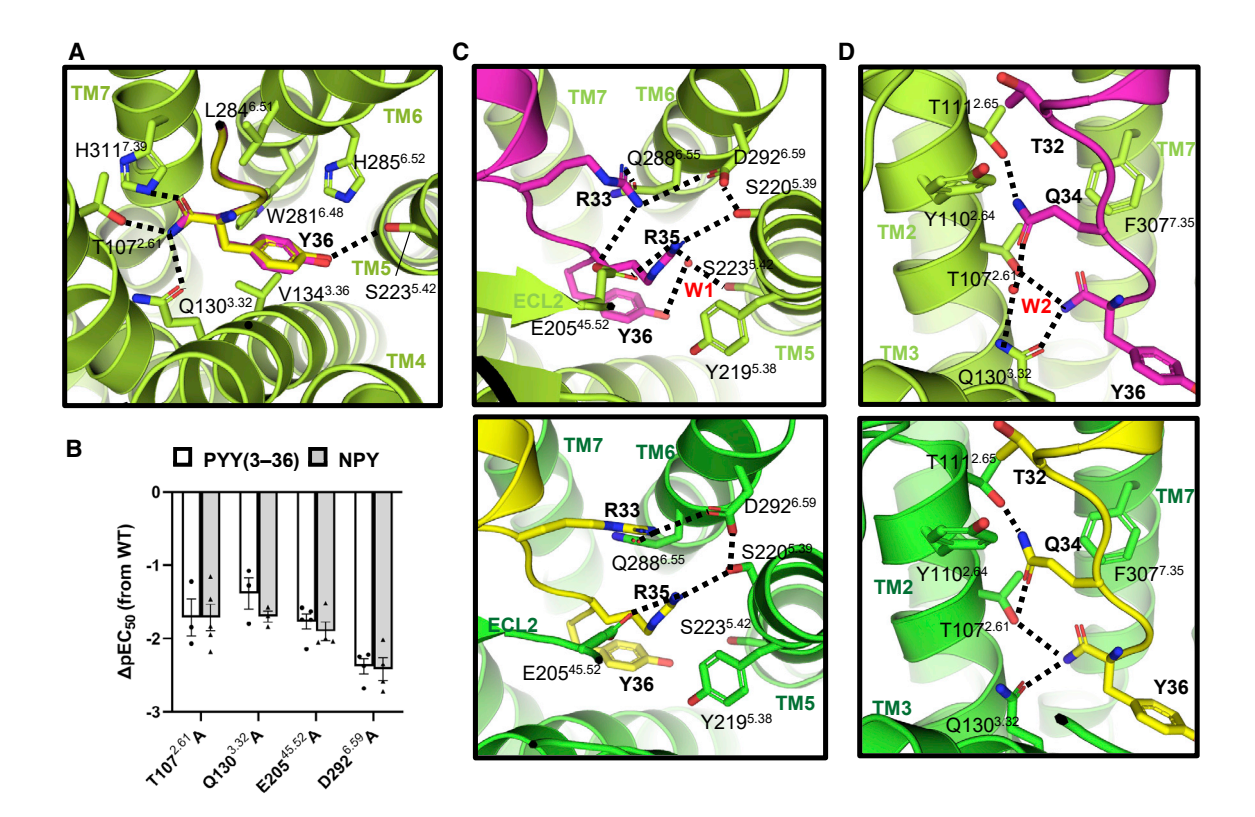


Figure 3. NPY/PYY(3-36) binding at the transmembrane domain of Y₂R (A) Interactions established by Y36 of NPY/PYY(3–36). The C-terminal amide group forms polar interactions with T107^{2.61}, Q130^{3.32}, and H311^{7.39}. The phenyl group forms van der Waals interactions with G131^{3,33}, V134^{3,36}, W281^{6,48}, L284^{6,51}, and H285^{6,52}. The hydroxyl group forms a polar interaction with S223^{5,42}. (B) Differences in pEC₅₀ for each Ala mutant of residues T107^{2.61}, Q130^{3.32}, E205^{45.52}, and D292^{6.59} relative to wild-type Y₂R. Values for treatment of PYY(3–36) and NPY are shown in white and gray bar graphs, respectively. Bar graphs and error bars indicate means and SEMs obtained from independent experiments (represented as symbols) of Ca²⁺ signaling assays, respectively. See also Figure S2. (C) Detailed interactions established by R33 and R35. A polar network is formed by $E205^{45.52}$, $S220^{5.39}$, $Q288^{6.55}$, and $D292^{6.59}$. In the PYY(3–36) – Y₂R structure (top), a water molecule (W1) interacting with R35 forms an extended polar network with Y36 and S223^{5.42}. (D) Detailed interactions established by T32 and Q34. These residues form polar and van der Waals interactions with T107^{2.61}, Y110^{2.64}, T111^{2.65}, and F307^{7.35}. In

the PYY(3-36)-Y₂R structure (top), a water molecule (W2) interacting with Q34 forms an extended polar network with Q130^{3.32}.

and angiotensin II type 1 and 2 receptors (AT₁R and AT₂R) bound to angiotensin. 37,38 In these complexes, the ligands occupy similar positions in the receptor subtypes.

Conserved interactions of NPY with Y1R and Y2R are associated with Y36-amide interactions with Q^{3.32} and H^{7.39} (Figure 4B). In addition, Y^{2.64} is located between T32 and Q34 and establishes contacts with these residues in both structures, despite their different positions in the two complexes (Figure 4B). Similarly, while R33 and R35 are located at different positions in the two structures, they form conserved polar interactions with Q/N^{6.55} and S/T^{5.39}, respectively (Figure 4B). In addition, D^{6.59} was identified as a key residue for NPY-induced signaling by forming electrostatic interactions with R33 in Y₂R and R35 in Y₁R.

In contrast to the conserved interactions of Y36-amide, the Y36 side-chain interactions are not conserved, as Q^{5.46} in Y₁R, which forms polar interaction with the hydroxyl group of Y36, is replaced with $\mathsf{L}^{5.46}$ in $\mathsf{Y}_2\mathsf{R},$ which cannot form polar interaction (Figure 4C). Instead, Y_2R S^{5.42}, but not Y_1R L^{5.42}, forms polar interaction with the hydroxyl group of Y36 (Figure 4C). Another distinct feature of NPY-Y2R interactions is the absence of an

aromatic residue at position 6.58 in Y_2R . Whereas Y_1R F286^{6.58} forms a π -cation interaction with R33, Y₂R has a Val at this position, which does not participate in the NPY interactions (Figure 4D). The V291^{6.58}F mutation of Y₂R resulted in a 10-fold reduction in NPY signaling (Figure S2, and Table S1), suggesting that the introduction of Phe at position 6.58 in Y₂R disturbed the Y₂R-specific ligand interaction network. The presence or absence of an aromatic residue at position 6.58 alters the R33 position and, consequently, the interaction network between the receptor and R33/R35 of NPY, so R33-D $^{6.59}$ and R35-E^{45.52} ionic pairs and R33-F^{6.58} and R35-D^{6.59} interaction pairs are formed in Y₂R and Y₁R, respectively (Figure 4D). At the extracellular region, only a small fraction of the Y₁R ECL2 (P183^{ECL2}, F184^{ECL2}) participate in the NPY interactions (Figure 4E). In contrast, the hydrophobic residues (I192^{ECL2}, I194^{ECL2}, I195^{ECL2}, and I200^{ECL2}) of Y₂R ECL2 are important for NPY recognition; these residues are not conserved in other NPY receptor subtypes, making it a distinct feature of NPY recognition by Y₂R.

Reactivity to the N-terminally truncated form of NPY/PYY distinguishes Y₂R from Y₁R.²³ In the previously published

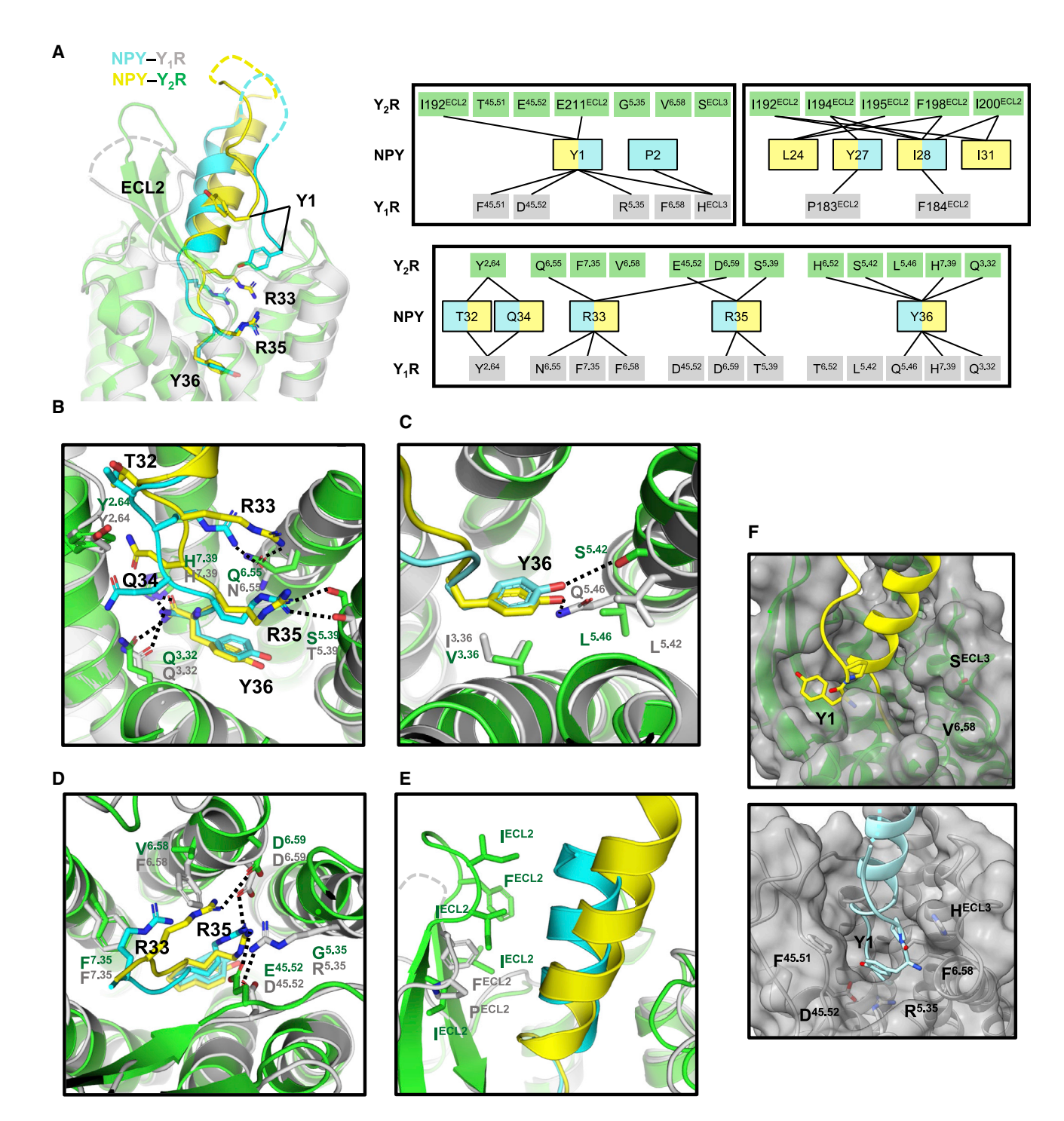


Figure 4. Structure comparison between NPY-bound Y₁R and Y₂R

(A) Superposition of NPY bound to Y₁R (Y₁R: gray, NPY: cyan; PDB: 7VGX) and Y₂R (Y₂R: green, NPY: yellow). Missing residues are represented as dashed lines. Schematic diagram of the main interactions between NPY and Y1R/Y2R is presented on the right, with the same color codes as in the overall superposition figure on the left. Each solid line represents the interaction between two residues.

- (B) Conserved NPY interactions with Y_1R and Y_2R . Interactions of the NPY C-tail with $Y^{2.64}$, $Q^{3.32}$, $S/T^{5.39}$, $Q/N^{6.55}$, and $H^{7.39}$ are conserved in the two structures. Polar contacts are displayed as dotted lines. Interacting residues of NPY, Y1R, and Y2R are labeled in black, gray, and dark green, respectively.
- (C) Comparison of the interactions of Y36 side chain with Y₁R and Y₂R. Y36 hydroxyl group forms a polar interaction with Q^{5,46} in Y₁R but not with the corresponding residue L^{5.46} in Y₂R. Instead, S^{5.42} in Y₂R forms polar contact with the Y36 side chain.
- (D) Interaction network formed by R33 and R35 of NPY. In Y₁R, F^{6.58} and D^{6.59} interact with R33 and R35, respectively, whereas in Y₂R, D^{6.59} and E^{45.52} form electrostatic interactions with R33 and R35, respectively.

Article



NPY-Y₁R structure, the binding pocket for Y1 and P2 was formed by F199^{45.51}, D200^{45.52}, R208^{5.35}, and F286^{6.58} of Y_1R (Figure 4F). In contrast, the corresponding residues in Y2R have smaller side chains (T204^{45.51}, E205^{45.52}, G216^{5.35}, and V291^{6.58}), making the pocket too wide to accommodate Y1 of NPY. Furthermore, owing to steric hindrance by Y27 and L30 of the NPY helix, the NPY N terminus cannot occupy the same position as in the NPY-Y₁R structure. As a result, in the NPYbound Y₁R and Y₂R structures, the NPY N termini are located 9.6 Å apart (Figure 4A). Y₂R has an ECL2-mediated hydrophobic interaction with the NPY helical region, leading to the stable binding of the NPY helix to Y2R; in contrast, Y1R lacks this ECL2-mediated interaction, causing the NPY helix to bind relatively loosely to the receptor.²¹

Potency of NPY/PYY for downstream transducer coupling in Y₁R and Y₂R

In addition to structural analysis of the NPY/PYY binding modes to Y₁R and Y₂R, we further investigated whether these receptors exhibit differences in downstream signaling upon NPY/PYY binding. Calcium signaling assays showed that Y₂R has a 4.5-fold lower EC_{50} value for NPY than that of Y_1R (0.98 vs. 4.4 nM) (Figure S2 and Table S1). However, a Gi recruitment assay using BRET showed that Y2R displays EC50 values similar to Y1R upon treatment of NPY/PYY (Figures 5A and S2 and Table S2). These results suggest that NPY/PYY exhibits similar potency at Y2R and Y1R in Gi signaling. Most of the Gα_i binding interfaces in Y₁R and Y₂R are conserved, including a hydrophobic interface consisting of residues $I^{3.54}$, $I^{5.61}$, $L^{5.65}$, $H^{5.68}$, and $L^{6.37}$ of TM3/TM5/TM6 and hydrophobic residues of Ga; a5-helix (Figure S6). At the Y2R-Ga; interface, additional interactions were observed: Y2596.27 and R261^{6.29} of Y_2R interact with F354 of $G\alpha_i$, and H249^{5.68} and P252^{5.71} of the ICL3 interact with Y320, F334, D337, D341, and I344 of $G\alpha_i$ (Figure S6).

In general, GPCRs activate β-arrestin-mediated signaling as well as G protein signaling upon agonist stimulation, one pathway can be preferentially activated over the other in some cases. Using BRET assay, we observed that both G_i and β-arrestin 2 were recruited to Y_1R and Y_2R after stimulation with 1 μM NPY/PYY. However, dose-dependent BRET assays on G_i and β -arrestin 2 recruitment showed a difference in the potency of NPY/PYY for downstream transducer coupling of each receptor. While Y1R displayed 1.7- to 2.4-fold difference in EC₅₀ values for G_i and β -arrestin 2 recruitment, Y2R showed a much larger difference in EC₅₀ for G_i and β -arrestin 2 coupling, i.e., an 8.4- to 13-fold higher EC₅₀ value for β -arrestin 2 coupling (Figure 5B and Table S2). These data show that NPY/PYY is more potent at Y₁R than at Y₂R in β-arrestin 2 signaling. This result is in line with a previous report that showed a higher affinity of Y₁R toward β-arrestin 2 than Y2R, which is thought to be due to the presence of six potential phosphorylation sites (residues 353, 354, 357, 360, 362, and 363) recognized by β-arrestin in the C-terminal region of Y₁R.³⁹

We speculated whether residue(s) other than the C-terminal phosphorylation sites could alter the balance between the G protein- and β-arrestin-mediated pathways. A recent structural analysis of sphingosine-1-phosphate receptor 1 in complex with unbiased and biased ligands suggested that the interaction network involving residues at positions 3.40, 3.43, 6.44, and 7.49 drives a conformational shift to favor the β-arrestin signaling pathway. Interestingly, Y₁R has an Ile at position 3.40 (I128^{3.40}) that forms a hydrophobic network with F272^{6.44} and P223^{5.50}, whereas Y₂R has a Thr (T138^{3.40}) that does not make close contacts with F277^{6.44} (Figure 5C). However, the substitution of T138^{3.40} with IIe (T138^{3.40}I) in Y_2R did not show significant changes in both G_i and β-arrestin-mediated pathways (Figure 5B and Table S2).

We introduced two other mutations in ${\rm H}155^{\rm ICL2}$ and ${\rm T}266^{6.33}$ of Y₂R, which are not conserved in Y₁R. The structural alignment between Y₁R and Y₂R revealed that both residues are at the G_i binding interface as well as at the potential β-arrestin binding interface. When each residue was mutated to the corresponding residue of Y_1R -i.e., $H155^{ICL2}P$ and $T266^{6.33}I$ - only the $H155^{ICL2}P$ mutant differed from the wild-type in its preference for G protein or β -arrestin 2 recruitment. This mutant showed enhanced β -arrestin 2 recruitment upon activation (3.5-fold), whereas G protein recruitment was similar to that of the wild-type (Figures 5B and 5C and Table S2). This result is in line with previous reports that H155^{ICL2}P enhances β-arrestin 2 recruitment.³⁹⁻⁴¹ Notably, H155^{ICL2}P Y₂R exhibits an EC₅₀ value similar to Y₁R for β-arrestin signaling. To understand the enhanced β-arrestin 2 recruitment of this mutant at the molecular level, we aligned our structure with those of two GPCR-β-arrestin complexes, neurotensin receptor 1 (NTS1R)- β -arrestin 1 (PDB: 6UP7) and β_1 adrenergic receptor (β₁AR)-β-arrestin 1 (PDB: 6TKO); two structures show different β-arrestin 1 binding poses. P^{ICL2} of NTS1R and β₁AR form an extensive hydrophobic network with Y63 and F75 at the edge of the finger loop and with L243 and F244 in the C-loop of β -arrestin 1 (Figure 5D). Thus, the H155^{ICL2}P mutation in Y₂R could enhance β-arrestin binding without affecting G protein interactions.

DISCUSSION

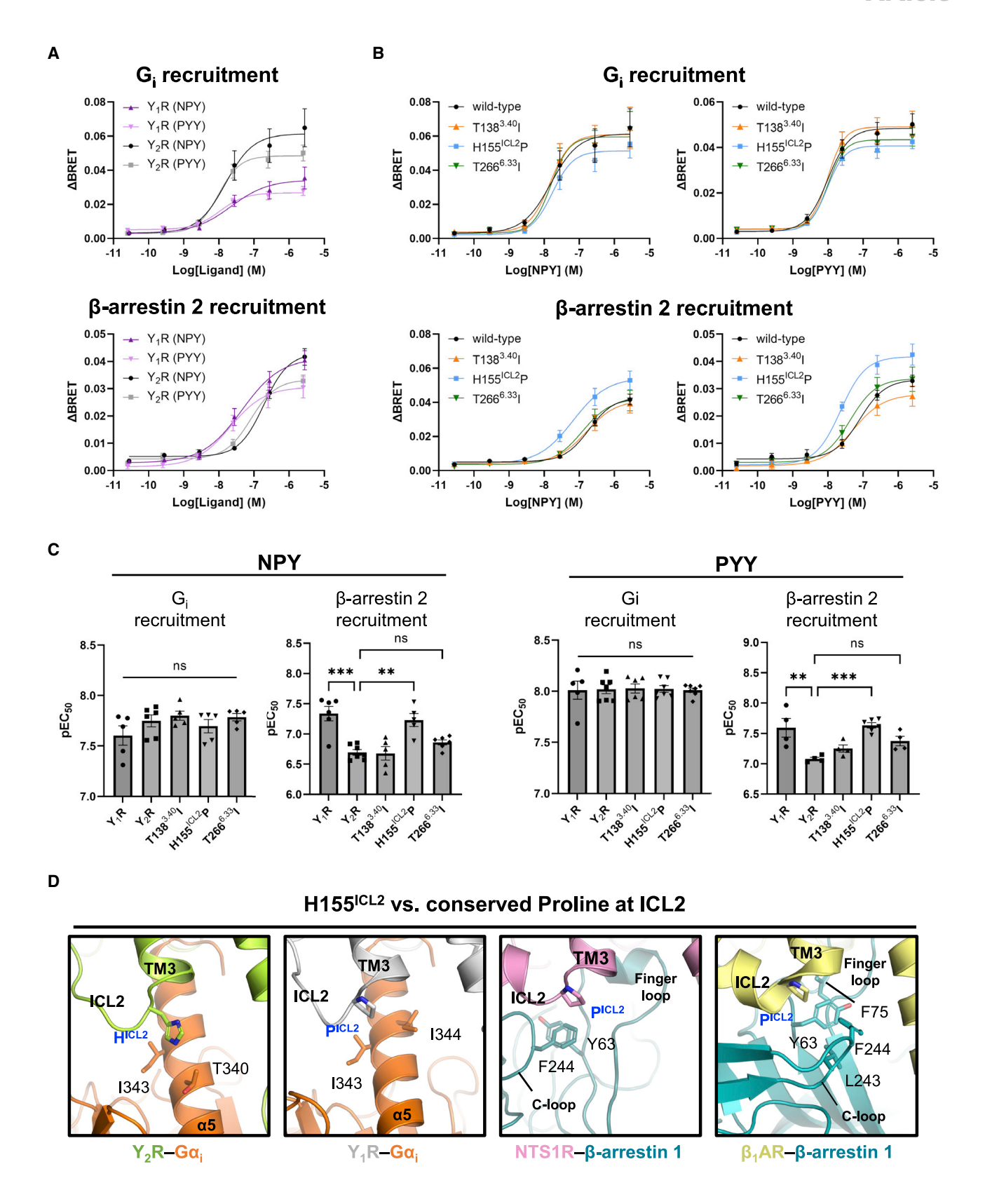
Unlike Y₁R, Y₂R can tolerate the N-terminal truncation of NPY/ PYY for downstream signaling. Using ITC, we have shown that the N-terminal truncation of NPY does not affect its binding affinity to Y₂R. Consistent with these data, the cryo-EM structures of NPY-Y₂R-G_i and PYY(3-36)-Y₂R-G_i complexes presented in this study show that the helical and C-terminal regions of the ligand form key interactions with the ECL2 and TMD of Y2R, respectively, whereas the N-terminal region does not directly contribute to Y2R binding; rather, it forms intramolecular contacts with the helical region of NPY/PYY(3-36). When compared with the antagonist-bound Y₂R structure, agonist-bound Y₂R exhibits conventional conformational changes of class A GPCRs upon activation, including a large outward movement of cytoplasmic part of TM6. While we were preparing this manuscript, a cryo-EM structure of the NPY-Y₂R-G_i complex at 3.4 Å resolution was published.²² Structural comparison shows that our

⁽E) NPY helix interactions. Unlike Y₁R ECL2, Y₂R ECL2 forming a β-turn-β structure establishes an extensive hydrophobic network with the hydrophobic side of the NPY α -helix.

⁽F) Interaction of Y1-P2 of NPY. Y1R- and Y2R-bound NPY adopt different conformations at their N termini. Surface models of Y1R (bottom) and Y2R (top), shown in gray volume, reveal that Y1 of NPY binds into a pocket formed by labeled residues in Y1R, but no similar binding pocket is formed in Y2R.







(legend on next page)

Article



structure aligns well with this published one, with an RMSD of 1.1 Å for 302 Cα atoms of Y₂R; however, the NPY N-terminal region, especially the Y1 side chain, is positioned differently in the two structures (Figure S7). Since the N-terminal region does not make extensive contacts with Y₂R, it is not surprising that it may adopt various conformations.

Structural comparison between NPY-bound Y1R and Y2R reveals that both receptors not only share conserved interactions with NPY, but they also display distinct binding modes of NPY (Figure 6). The conserved interactions are mediated by the amidated C terminus of NPY that forms polar contacts with Q^{3.32} and H^{7.39}, both of which are conserved in the NPYR family. Except for Y36 and R35, most residues of NPY occupy different positions in Y1R and Y₂R, showing approximately a 2- to 3-Å shift of the C-terminal residues 32-34, a 2-Å shift of the whole helix, and a 9.6-Å shift of the N terminus. This is a fairly unique case of considerable differences in agonist recognition within the same GPCR family. Residues R33 and R35 of NPY, which were suggested as the most important amino acids for agonist potency, show a different interaction network in the two complex structures. This difference may arise from the absence or presence of a bulky aromatic residue at position 6.58. In the NPY-bound Y₁R structure, F^{6.58} forms a π -cation interaction with R33, whereas Y_2R $V^{6.58}$ does not participate in NPY binding. In addition, $Y_1R F^{6.\overline{5}8}$ was shown to interact with Y1 of NPY.²¹ Interestingly, amino acid at position 6.58 varies among NPYR subtypes: F^{6.58}, V^{6.58}, E^{6.58}, and T^{6.58} in Y₁R, Y₂R, Y₄R, and Y₅R, respectively. The cryo-EM structure of PP-bound Y_4R from a previous report²² and a prediction model of NPY-bound Y_5R proposed that $E^{6.58}/T^{6.58}$ interact with R33, suggesting that the residue at position 6.58 is responsible for the receptor subtype-specific interaction with R33, except for V^{6.58} of Y₂R (Figure S7). Another distinct feature of NPY/PYY recognition by Y₂R occurs in the Ile-rich region of the ECL2. In contrast to the flexible Y₁R ECL2, which is associated with the dynamic motion of the NPY helix in the NPY-Y₁R structure, the Y₂R ECL2 establishes a hydrophobic interaction network with NPY, making its helix relatively rigidly bound to the receptor, as demonstrated by MD simulations. The lack of ECL2-mediated extensive hydrophobic interactions with the NPY helix in the NPY-Y₁R complex appears to be compensated by the interaction of Y₁R with the NPY N terminus, which consequently results in similar NPY potencies at Y1R and Y₂R.

GPCR subtypes activated by the same agonist can exhibit different G protein-coupling selectivity or downstream regulator selectivity between β-arrestin and G protein. For example, galanin receptors 1 and 2 exhibit different G protein-coupling selectivity by activating \boldsymbol{G}_{i} and \boldsymbol{G}_{q} signaling, respectively, when stimulated by galanin. 42 On the other hand, noradrenaline shows a similar potency to β_1AR and β_2AR for G protein-coupling but a high potency to $\beta_1 AR$ for $\beta\text{-arrestin-coupling.}^{43}$ In the case of Y₁R and Y₂R, they both activate Gi signaling upon NPY binding but show a different coupling efficiency with G protein and β-arrestin, i.e., Y_1R activation by NPY/PYY transmits G_i and β -arrestin signaling with similar efficiency, but Y₂R activation favors G_i signaling over β -arrestin signaling (Figure 6). A previous report has shown that Y_1R has a high affinity for β -arrestin 2 and forms a supercomplex with $\beta\text{-arrestin 2}$ and $G\alpha_o.^{39}$ It was suggested that the C-terminal tail of Y₁R is responsible for this high binding affinity, based on the presence of multiple possible phosphorylation sites that can be recognized by β -arrestin 2. In our study, we designed three mutations of Y₂R based on structural comparison with Y₁R, T^{3.40}I, H^{ICL2}P, and T^{6.33}I, but only the H^{ICL2}P mutant showed enhanced β -arrestin signaling without affecting G protein signaling, suggesting that Pro residue at this position affects preference for downstream pathways. Further studies are needed to understand how this change in downstream coupling selectivity relates to physiological responses. Together with structural data, downstream coupling selectivity will provide important information for the development of receptor subtypespecific biased ligands.

STAR*METHODS

Detailed methods are provided in the online version of this paper and include the following:

- KEY RESOURCES TABLE
- RESOURCE AVAILABILITY
 - Lead contact
 - Materials availability
 - Data and code availability
- EXPERIMENTAL MODEL AND SUBJECT DETAILS
- METHOD DETAILS
 - Expression and purification of Y₂R
 - Expression and purification of heterotrimeric G_i
 - Expression and purification of scFv16
 - Y₂R complex purification
 - Cryo-EM grid preparation and data collection
 - Cryo-EM data processing
 - Model building and refinement
 - Molecular dynamics simulation
 - Isothermal titration calorimetry

Figure 5. Differences in downstream G protein/β-arrestin recruitment between Y₁R, Y₂R, and Y₂R mutants

(A) NPY/PYY-induced G_i (top) and β-arrestin 2 (bottom) recruitment to Y₁R and Y₂R were measured using bioluminescence resonance energy transfer (BRET) assays. Δ BRET is calculated by the difference between ligand- and vehicle-treated BRET signals. The symbols and error bars represent the means and the SEM. The EC₅₀ values for each experiment are listed in Table S2.

(B) NPY/PYY-induced G_i(top) and β-arrestin 2 (bottom) recruitment to wild-type Y₂R and mutants Y₂R were measured using BRET assays. The symbols and error bars represent the means and the SEM. The EC₅₀ values for each experiment are listed in Table S2.

(C) pEC₅₀ data from BRET assays were subjected to one-way ANOVA followed by Tukey's test for statistical significance test. The bar graphs and error bars represent the means and the SEM of pEC50 calculated from independent experiments represented as symbols. Significance of each comparison is indicated as ns (p > 0.1), **p < 0.01, and ***p < 0.001.

(D) Structural analysis of H155 CL2P mutation of Y₂R. For structural comparison, NPY-Y₁R-G₁ (PDB: 7VGX), NTS-NTS1R-β-arrestin 1 (PDB: 6UP7), and for-and the interactions of corresponding Pro residues in Y_1R (gray) bound to G_i (orange), NTS1R (pink) bound to G_i -arrestin 1 (teal blue), and G_i -arrestin 1 (teal blu β -arrestin 1 (teal blue) are shown. H155^{ICL2} of Y₂R and corresponding P^{ICL2} of Y₁R, NTS1R, and β ₁AR are labeled in bold blue.



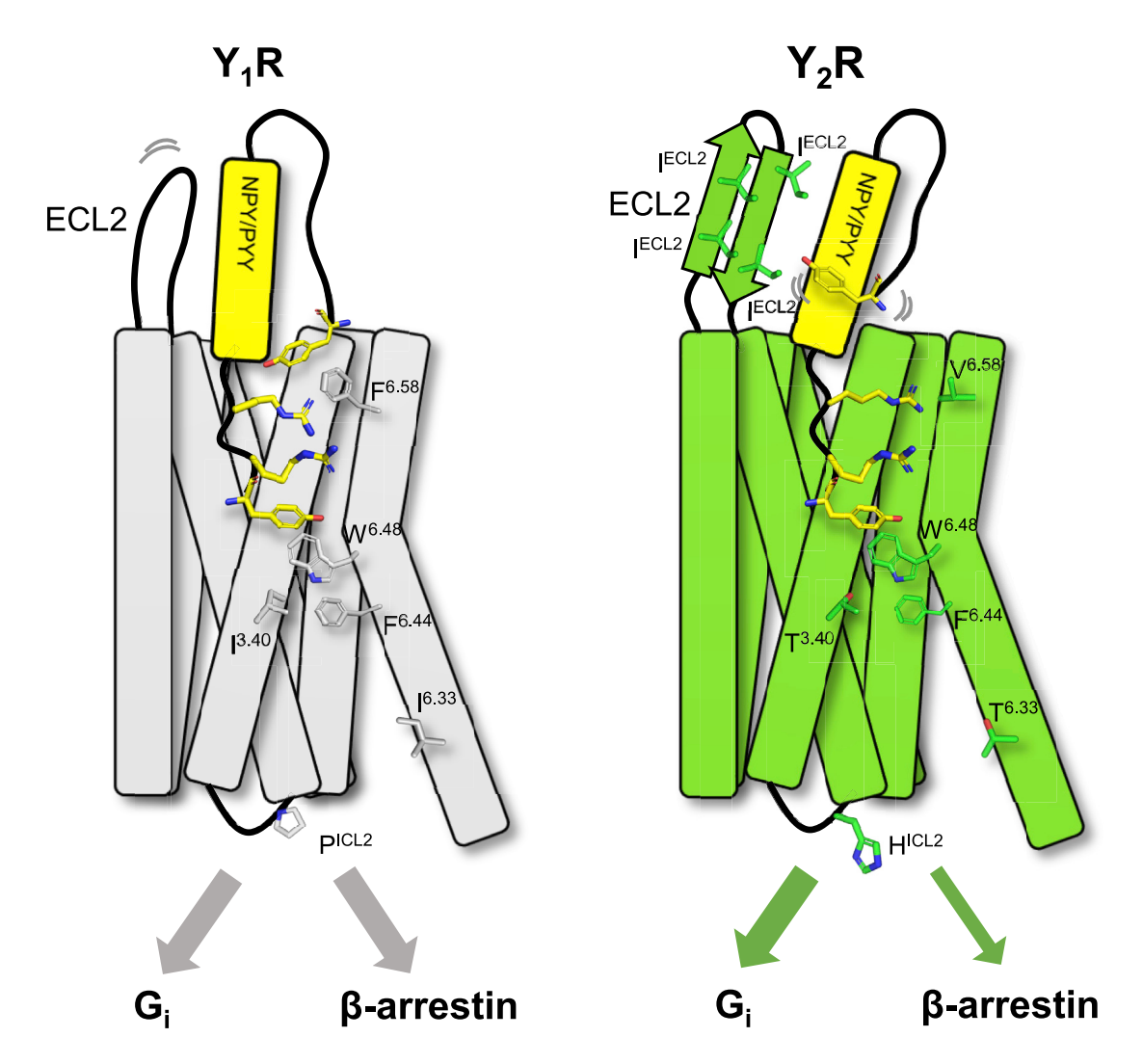


Figure 6. Schematic representation of NPY binding modes and downstream signaling in Y₁R and Y₂R

While Y_1R and Y_2R are activated by the same endogenous agonists, NPY/PYY, the agonist peptide binding mode is not conserved in the two receptors, displaying critical differences in NPY/PYY recognition. Key residues in Y_1R and Y_2R showing differences in NPY/PYY recognition and downstream signaling are shown as stick figures. Each downstream G_1/β -arrestin signaling is represented as an arrow, with a thicker arrow meaning the better recruitment efficiency of the signaling molecule.

- BRET assay
- O ELISA-based surface expression assay
- Ca²⁺ signaling assay
- Modeling of NPY-bound Y₅R
- QUANTIFICATION AND STATISTICAL ANALYSIS

SUPPLEMENTAL INFORMATION

Supplemental information can be found online at https://doi.org/10.1016/j.str. 2022.11.010.

ACKNOWLEDGMENTS

We thank Dr. Seong-Gyu Lee and Dr. Burn Han Ryu (Institute for Basic Science, IBS, Korea) for supporting data collection at IBS cryo-EM facilities. We also thank Global Science experimental Data hub Center (GSDC) at Korea Institute of Science and Technology Information (KISTI) and the data analysis hub, Olaf at the IBS Research Solution Center for computing resources and technical support. Financial supports were provided by the National Research Foundation of Korea

funded by the Korean government (NRF-2020R1A2C2003783 and NRF-2019M3E5D6063903 to H.-J.C.), and National Science Foundation, USA (MCB-2111728 to W.I.).

AUTHOR CONTRIBUTIONS

Conceptualization, H.K., C.P., and H.-J.C. Methodology, H.K., Y.K.C., S.K., and H.-J.C. Investigation, H.K., C.P., Y.K.C., J.B., S.K., and C.C. Validation, J.B. and J.K. Visualization, H.K., C.P., and Y.K.C. Writing – original draft, H.K., C.P., and H.-J.C. Funding acquisition, W.I. and H.-J.C. Supervision, C.S., W.I., and H.-J.C. Project administration, H.-J.C.

DECLARATION OF INTERESTS

The authors declare no competing interests.

INCLUSION AND DIVERSITY

We support inclusive, diverse, and equitable conduct of research.

Article

CellPress

Received: October 26, 2022 Revised: November 6, 2022 Accepted: November 18, 2022 Published: December 15, 2022

REFERENCES

- 1. Yi, M., Li, H., Wu, Z., Yan, J., Liu, Q., Ou, C., and Chen, M. (2018). A promising therapeutic target for metabolic diseases: neuropeptide Y receptors in humans. Cell. Physiol. Biochem. 45, 88-107. https://doi.org/10.1159/
- 2. Baldock, P.A., Lee, N.J., Driessler, F., Lin, S., Allison, S., Stehrer, B., Lin, E.J.D., Zhang, L., Enriquez, R.F., Wong, I.P.L., et al. (2009). Neuropeptide Y knockout mice reveal a central role of NPY in the coordination of bone mass to body weight. PLoS One 4, e8415. https://doi.org/ 10.1371/journal.pone.0008415.
- 3. Tasan, R.O., Verma, D., Wood, J., Lach, G., Hörmer, B., de Lima, T.C.M., Herzog, H., and Sperk, G. (2016). The role of Neuropeptide Y in fear conditioning and extinction. Neuropeptides 55, 111-126. https://doi.org/10. 1016/j.npep.2015.09.007.
- 4. Gøtzsche, C.R., and Woldbye, D.P.D. (2016). The role of NPY in learning and memory. Neuropeptides 55, 79-89. https://doi.org/10.1016/j.npep. 2015.09.010.
- 5. Flood, J.F., and Morley, J.E. (1991). Increased food intake by neuropeptide Y is due to an increased motivation to eat. Peptides 12, 1329-1332. https://doi.org/10.1016/0196-9781(91)90215-b.
- 6. Lin, S.T., Li, Y.Z., Sun, X.Q., Chen, Q.Q., Huang, S.F., Lin, S., and Cai, S.Q. (2021). Update on the role of neuropeptide Y and other related factors in breast cancer and osteoporosis. Front. Endocrinol. 12, 705499. https:// doi.org/10.3389/fendo.2021.705499.
- 7. Chen, X.Y., Du, Y.F., and Chen, L. (2018). Neuropeptides exert neuroprotective effects in Alzheimer's disease. Front. Mol. Neurosci. 11, 493. https://doi.org/10.3389/fnmol.2018.00493.
- 8. Yulyaningsih, E., Zhang, L., Herzog, H., and Sainsbury, A. (2011). NPY receptors as potential targets for anti-obesity drug development. Br. J. Pharmacol. 163, 1170-1202. https://doi.org/10.1111/j.1476-5381.2011. 01363.x.
- 9. Reichmann, F., and Holzer, P. (2016). Neuropeptide Y: a stressful review. Neuropeptides 55, 99-109. https://doi.org/10.1016/j.npep.2015.09.008.
- 10. Ekblad, E., and Sundler, F. (2002). Distribution of pancreatic polypeptide and peptide YY. Peptides 23, 251-261. https://doi.org/10.1016/S0196-9781(01)00601-5.
- 11. Kojima, S., Ueno, N., Asakawa, A., Sagiyama, K., Naruo, T., Mizuno, S., and Inui, A. (2007). A role for pancreatic polypeptide in feeding and body weight regulation. Peptides 28, 459-463. https://doi.org/10.1016/j.peptides.2006.09.024.
- 12. Karra, E., Chandarana, K., and Batterham, R.L. (2009). The role of peptide YY in appetite regulation and obesity. J. Physiol. 587, 19-25. https://doi. org/10.1113/jphysiol.2008.164269.
- 13. Pedragosa-Badia, X., Stichel, J., and Beck-Sickinger, A.G. (2013). Neuropeptide Y receptors: how to get subtype selectivity. Front. Endocrinol. 4, 5. https://doi.org/10.3389/fendo.2013.00005.
- 14. Grandt, D., Schimiczek, M., Rascher, W., Feth, F., Shively, J., Lee, T.D., Davis, M.T., Reeve, J.R., Jr., and Michel, M.C. (1996). Neuropeptide Y 3-36 is an endogenous ligand selective for Y2 receptors. Regul. Pept. 67, 33-37. https://doi.org/10.1016/s0167-0115(96)00104-8.
- 15. Gerald, C., Walker, M.W., Criscione, L., Gustafson, E.L., Batzl-Hartmann, C., Smith, K.E., Vaysse, P., Durkin, M.M., Laz, T.M., Linemeyer, D.L., et al. (1996). A receptor subtype involved in neuropeptide-Y-induced food intake. Nature 382, 168-171. https://doi.org/10.1038/382168a0.
- 16. Batterham, R.L., Cowley, M.A., Small, C.J., Herzog, H., Cohen, M.A., Dakin, C.L., Wren, A.M., Brynes, A.E., Low, M.J., Ghatei, M.A., et al. (2002). Gut hormone PYY₃₋₃₆ physiologically inhibits food intake. Nature 418, 650-654. https://doi.org/10.1038/nature00887.

- 17. Lin, S., Boey, D., and Herzog, H. (2004). NPY and Y receptors: lessons from transgenic and knockout models. Neuropeptides 38, 189-200. https://doi.org/10.1016/j.npep.2004.05.005.
- 18. Müller, T.D., Blüher, M., Tschöp, M.H., and DiMarchi, R.D. (2022). Antiobesity drug discovery: advances and challenges. Nat. Rev. Drug Discov. 21, 201-223. https://doi.org/10.1038/s41573-021-00337-8.
- 19. Lu, C., Everhart, L., Tilan, J., Kuo, L., Sun, C.C.J., Munivenkatappa, R.B., Jönsson-Rylander, A.C., Sun, J., Kuan-Celarier, A., Li, L., et al. (2010). Neuropeptide Y and its Y2 receptor: potential targets in neuroblastoma therapy. Oncogene 29, 5630-5642. https://doi.org/10.1038/onc.2010.301.
- 20. Ahrens, V.M., Frank, R., Stadlbauer, S., Beck-Sickinger, A.G., and Hey-Hawkins, E. (2011). Incorporation of ortho-carbaboranyl-N_s-modified I-lysine into neuropeptide Y receptor Y₁- and Y₂-selective analogues. J. Med. Chem. 54, 2368-2377. https://doi.org/10.1021/jm101514m.
- 21. Park, C., Kim, J., Ko, S.B., Choi, Y.K., Jeong, H., Woo, H., Kang, H., Bang, I., Kim, S.A., Yoon, T.Y., et al. (2022). Structural basis of neuropeptide Y signaling through Y₁ receptor. Nat. Commun. 13, 853. https://doi.org/10. 1038/s41467-022-28510-6.
- 22. Tang, T., Tan, Q., Han, S., Diemar, A., Löbner, K., Wang, H., Schüß, C., Behr, V., Mörl, K., Wang, M., et al. (2022). Receptor-specific recognition of NPY peptides revealed by structures of NPY receptors. Sci. Adv. 8, eabm1232. https://doi.org/10.1126/sciadv.abm1232.
- 23. Beck-Sickinger, A.G., and Jung, G. (1995). Structure-activity relationships of neuropeptide Y analogues with respect to Y1 and Y2 receptors. Biopolymers 37, 123-142. https://doi.org/10.1002/bip.360370207.
- 24. Ballesteros, J.A., and Weinstein, H. (1995). Integrated methods for the construction of three-dimensional models and computational probing of structure-function relations in G protein-coupled receptors. Methods Neurosci. 25, 366-428. https://doi.org/10.1016/S1043-9471(05)80049-7.
- 25. Tang, T., Hartig, C., Chen, Q., Zhao, W., Kaiser, A., Zhang, X., Zhang, H., Qu, H., Yi, C., Ma, L., et al. (2021). Structural basis for ligand recognition of the neuropeptide YY₂ receptor. Nat. Commun. 12, 737. https://doi.org/10. 1038/s41467-021-21030-9.
- 26. Weis, W.I., and Kobilka, B.K. (2018). The molecular basis of G proteincoupled receptor activation. Annu. Rev. Biochem. 87, 897-919. https:// doi.org/10.1146/annurev-biochem-060614-033910.
- 27. Hong, C., Byrne, N.J., Zamlynny, B., Tummala, S., Xiao, L., Shipman, J.M., Partridge, A.T., Minnick, C., Breslin, M.J., Rudd, M.T., et al. (2021). Structures of active-state orexin receptor 2 rationalize peptide and small-molecule agonist recognition and receptor activation. Nat. Commun. 12, 815. https://doi.org/10.1038/s41467-021-21087-6.
- 28. Bjørnholm, B., Jørgensen, F.S., and Schwartz, T.W. (1993). Conservation of a helix-stabilizing dipole moment in the PP-fold family of regulatory peptides. Biochemistry 32, 2954-2959. https://doi.org/10.1021/bi00063a005.
- 29. Nygaard, R., Nielbo, S., Schwartz, T.W., and Poulsen, F.M. (2006). The PPfold solution structure of human polypeptide YY and human PYY3-36 as determined by NMR. Biochemistry 45, 8350-8357. https://doi.org/10. 1021/bi060359l.
- 30. Li, X.A., Sutcliffe, M.J., Schwartz, T.W., and Dobson, C.M. (1992). Sequence-specific ¹H NMR assignments and solution structure of bovine pancreatic polypeptide. Biochemistry 31, 1245-1253. https://doi.org/10. 1021/bi00119a038.
- 31. Monks, S.A., Karagianis, G., Howlett, G.J., and Norton, R.S. (1996). Solution structure of human neuropeptide Y. J. Biomol. NMR 8, 379-390. https://doi.org/10.1007/BF00228141.
- 32. Saudek, V., and Pelton, J.T. (1990). Sequence-specific ¹H NMR assignment and secondary structure of neuropeptide Y in aqueous solution. Biochemistry 29, 4509-4515. https://doi.org/10.1021/bi00471a002.
- 33. Kaiser, A., Müller, P., Zellmann, T., Scheidt, H.A., Thomas, L., Bosse, M., Meier, R., Meiler, J., Huster, D., Beck-Sickinger, A.G., and Schmidt, P. (2015). Unwinding of the C-terminal residues of neuropeptide Y is critical for Y2 receptor binding and activation. Angew. Chem. Int. Ed. Engl. 54, 7446-7449. https://doi.org/10.1002/anie.201411688.





- Keire, D.A., Mannon, P., Kobayashi, M., Walsh, J.H., Solomon, T.E., and Reeve, J.R. (2000). Primary structures of PYY, [Pro³⁴]PYY, and PYY-(3–36) confer different conformations and receptor selectivity. Am. J. Physiol. Gastrointest. Liver Physiol. 279, G126–G131. https://doi.org/10. 1152/ajpgi.2000.279.1.G126.
- Xu, X., Kaindl, J., Clark, M.J., Hübner, H., Hirata, K., Sunahara, R.K., Gmeiner, P., Kobilka, B.K., and Liu, X. (2021). Binding pathway determines norepinephrine selectivity for the human β₁AR over β₂AR. Cell Res. 31, 569–579. https://doi.org/10.1038/s41422-020-00424-2.
- Ring, A.M., Manglik, A., Kruse, A.C., Enos, M.D., Weis, W.I., Garcia, K.C., and Kobilka, B.K. (2013). Adrenaline-activated structure of β₂-adrenoceptor stabilized by an engineered nanobody. Nature 502, 575–579. https://doi.org/10.1038/nature12572.
- Asada, H., Inoue, A., Ngako Kadji, F.M., Hirata, K., Shiimura, Y., Im, D., Shimamura, T., Nomura, N., Iwanari, H., Hamakubo, T., et al. (2020). The crystal structure of angiotensin II type 2 receptor with endogenous peptide hormone. Structure 28, 418–425.e4. https://doi.org/10.1016/j.str.2019. 12.003.
- Wingler, L.M., Skiba, M.A., McMahon, C., Staus, D.P., Kleinhenz, A.L.W., Suomivuori, C.M., Latorraca, N.R., Dror, R.O., Lefkowitz, R.J., and Kruse, A.C. (2020). Angiotensin and biased analogs induce structurally distinct active conformations within a GPCR. Science 367, 888–892. https://doi. org/10.1126/science.aay9813.
- Wanka, L., Babilon, S., Kaiser, A., Mörl, K., and Beck-Sickinger, A.G. (2018). Different mode of arrestin-3 binding at the human Y₁ and Y₂ receptor. Cell. Signal. 50, 58–71. https://doi.org/10.1016/j.cellsig.2018.06.010.
- Kilpatrick, L.E., Briddon, S.J., Hill, S.J., and Holliday, N.D. (2010). Quantitative analysis of neuropeptide Y receptor association with beta-arrestin2 measured by bimolecular fluorescence complementation. Br. J. Pharmacol. 160, 892–906. https://doi.org/10.1111/j.1476-5381.2010.00676.x.
- Ouedraogo, M., Lecat, S., Rochdi, M.D., Hachet-Haas, M., Matthes, H., Gicquiaux, H., Verrier, S., Gaire, M., Glasser, N., Mély, Y., et al. (2008). Distinct motifs of neuropeptide Y receptors differentially regulate trafficking and desensitization. Traffic 9, 305–324. https://doi.org/10.1111/j. 1600-0854.2007.00691.x.
- Duan, J., Shen, D.D., Zhao, T., Guo, S., He, X., Yin, W., Xu, P., Ji, Y., Chen, L.N., Liu, J., et al. (2022). Molecular basis for allosteric agonism and G protein subtype selectivity of galanin receptors. Nat. Commun. 13, 1364. https://doi.org/10.1038/s41467-022-29072-3.
- Casella, I., Ambrosio, C., Grò, M.C., Molinari, P., and Costa, T. (2011).
 Divergent agonist selectivity in activating β₁- and β₂-adrenoceptors for G-protein and arrestin coupling. Biochem. J. 438, 191–202. https://doi.org/10.1042/BJ20110374.
- Punjani, A., Rubinstein, J.L., Fleet, D.J., and Brubaker, M.A. (2017). cryoSPARC: algorithms for rapid unsupervised cryo-EM structure determination. Nat. Methods 14, 290–296. https://doi.org/10.1038/nmeth.4169.
- Pettersen, E.F., Goddard, T.D., Huang, C.C., Meng, E.C., Couch, G.S., Croll, T.I., Morris, J.H., and Ferrin, T.E. (2021). UCSF ChimeraX: structure visualization for researchers, educators, and developers. Protein Sci. 30, 70–82. https://doi.org/10.1002/pro.3943.
- Liebschner, D., Afonine, P.V., Baker, M.L., Bunkóczi, G., Chen, V.B., Croll, T.I., Hintze, B., Hung, L.W., Jain, S., McCoy, A.J., et al. (2019). Macromolecular structure determination using X-rays, neutrons and electrons: recent developments in Phenix. Acta Crystallogr. D Struct. Biol. 75, 861–877. https://doi.org/10.1107/S2059798319011471.
- Williams, C.J., Headd, J.J., Moriarty, N.W., Prisant, M.G., Videau, L.L., Deis, L.N., Verma, V., Keedy, D.A., Hintze, B.J., Chen, V.B., et al. (2018). MolProbity: more and better reference data for improved all-atom structure validation. Protein Sci. 27, 293–315. https://doi.org/10.1002/pro.3330.
- Barad, B.A., Echols, N., Wang, R.Y.R., Cheng, Y., DiMaio, F., Adams, P.D., and Fraser, J.S. (2015). EMRinger: side chain-directed model and map validation for 3D cryo-electron microscopy. Nat. Methods 12, 943–946. https://doi.org/10.1038/nmeth.3541.

- Emsley, P., Lohkamp, B., Scott, W.G., and Cowtan, K. (2010). Features and development of coot. Acta Crystallogr. D Biol. Crystallogr. 66, 486–501. https://doi.org/10.1107/S0907444910007493.
- Van Der Spoel, D., Lindahl, E., Hess, B., Groenhof, G., Mark, A.E., and Berendsen, H.J.C. (2005). GROMACS: fast, flexible, and free.
 J. Comput. Chem. 26, 1701–1718. https://doi.org/10.1002/jcc.20291.
- Humphrey, W., Dalke, A., and Schulten, K. (1996). VMD: visual molecular dynamics. J. Mol. Graph. 14, 33–38. 27-28. https://doi.org/10.1016/0263-7855(96)00018-5.
- Jo, S., Kim, T., Iyer, V.G., and Im, W. (2008). CHARMM-GUI: a web-based graphical user interface for CHARMM. J. Comput. Chem. 29, 1859–1865. https://doi.org/10.1002/jcc.20945.
- Evans, R., O'Neill, M., Pritzel, A., Antropova, N., Senior, A., Green, T., Žídek, A., Bates, R., Blackwell, S., Yim, J., et al. (2022). Protein complex prediction with AlphaFold-Multimer. Preprint at bioRxiv. https://doi.org/ 10.1101/2021.10.04.463034.
- Heo, L., Lee, H., and Seok, C. (2016). GalaxyRefineComplex: refinement of protein-protein complex model structures driven by interface repacking. Sci. Rep. 6, 32153. https://doi.org/10.1038/srep32153.
- Lee, G.R., and Seok, C. (2016). Galaxy7TM: flexible GPCR-ligand docking by structure refinement. Nucleic Acids Res. 44, W502–W506. https://doi. org/10.1093/nar/gkw360.
- Choi, H.K., Min, D., Kang, H., Shon, M.J., Rah, S.H., Kim, H.C., Jeong, H., Choi, H.J., Bowie, J.U., and Yoon, T.Y. (2019). Watching helical membrane proteins fold reveals a common N-to-C-terminal folding pathway. Science 366, 1150–1156. https://doi.org/10.1126/science.aaw8208.
- 57. Maeda, S., Koehl, A., Matile, H., Hu, H., Hilger, D., Schertler, G.F.X., Manglik, A., Skiniotis, G., Dawson, R.J.P., and Kobilka, B.K. (2018). Development of an antibody fragment that stabilizes GPCR/G-protein complexes. Nat. Commun. 9, 3712. https://doi.org/10.1038/s41467-018-06002-w.
- Asarnow, D., Palovcak, E., and Cheng, Y. (2019). Asarnow/Pyem: UCSF Pyem v0.5.
- Kang, Y., Kuybeda, O., de Waal, P.W., Mukherjee, S., Van Eps, N., Dutka, P., Zhou, X.E., Bartesaghi, A., Erramilli, S., Morizumi, T., et al. (2018). Cryo-EM structure of human rhodopsin bound to an inhibitory G protein. Nature 558, 553–558. https://doi.org/10.1038/s41586-018-0215-y.
- Huang, J., Rauscher, S., Nawrocki, G., Ran, T., Feig, M., de Groot, B.L., Grubmüller, H., and MacKerell, A.D., Jr. (2017). CHARMM36m: an improved force field for folded and intrinsically disordered proteins. Nat. Methods 14, 71–73. https://doi.org/10.1038/nmeth.4067.
- Klauda, J.B., Venable, R.M., Freites, J.A., O'Connor, J.W., Tobias, D.J., Mondragon-Ramirez, C., Vorobyov, I., MacKerell, A.D., Jr., and Pastor, R.W. (2010). Update of the CHARMM all-atom additive force field for lipids: validation on six lipid types. J. Phys. Chem. B *114*, 7830–7843. https://doi. org/10.1021/jp101759g.
- Klauda, J.B., Monje, V., Kim, T., and Im, W. (2012). Improving the CHARMM force field for polyunsaturated fatty acid chains. J. Phys. Chem. B 116, 9424–9431. https://doi.org/10.1021/jp304056p.
- Jo, S., Kim, T., and Im, W. (2007). Automated builder and database of protein/membrane complexes for molecular dynamics simulations. PLoS One 2, e880. https://doi.org/10.1371/journal.pone.0000880.
- 64. Jo, S., Lim, J.B., Klauda, J.B., and Im, W. (2009). CHARMM-GUI Membrane Builder for mixed bilayers and its application to yeast membranes. Biophys. J. 97, 50–58. https://doi.org/10.1016/j.bpj.2009.04.013.
- Lee, J., Cheng, X., Swails, J.M., Yeom, M.S., Eastman, P.K., Lemkul, J.A., Wei, S., Buckner, J., Jeong, J.C., Qi, Y., et al. (2016). CHARMM-GUI input generator for NAMD, GROMACS, AMBER, OpenMM, and CHARMM/ OpenMM simulations using the CHARMM36 additive force field. J. Chem. Theory Comput. 12, 405–413. https://doi.org/10.1021/acs.jctc. 5500935
- 66. Hess, B., Bekker, H., Berendsen, H.J.C., and Fraaije, J.G.E.M. (1997). LINCS: a linear constraint solver for molecular simulations. J. Comput. Chem. 18, 1463–1472. https://doi.org/10.1002/(SICI)1096-987X(199709) 18:12<1463::AID-JCC4>3.0.CO;2-H.

Article



- 67. Steinbach, P.J., and Brooks, B.R. (1994). New spherical-cutoff methods for long-range forces in macromolecular simulation. J. Comput. Chem. 15, 667-683. https://doi.org/10.1002/jcc.540150702.
- 68. Essmann, U., Perera, L., Berkowitz, M.L., Darden, T., Lee, H., and Pedersen, L.G. (1995). A smooth particle mesh Ewald method. J. Chem. Phys. 103, 8577-8593. https://doi.org/10.1063/1.470117.
- 69. Parrinello, M., and Rahman, A. (1981). Polymorphic transitions in single crystals: a new molecular dynamics method. J. Appl. Phys. 52, 7182-7190. https://doi.org/10.1063/1.328693.
- 70. Hopkins, C.W., Le Grand, S., Walker, R.C., and Roitberg, A.E. (2015). Long-time-step molecular dynamics through hydrogen mass repartition-
- ing. J. Chem. Theory Comput. 11, 1864-1874. https://doi.org/10.1021/ ct5010406.
- 71. Galés, C., Van Durm, J.J.J., Schaak, S., Pontier, S., Percherancier, Y., Audet, M., Paris, H., and Bouvier, M. (2006). Probing the activation-promoted structural rearrangements in preassembled receptor-G protein complexes. Nat. Struct. Mol. Biol. 13, 778-786. https://doi.org/10.1038/ nsmb1134.
- 72. Kostenis, E. (2002). Potentiation of GPCR-signaling via membrane targeting of G protein alpha subunits. J. Recept. Signal Transduct. Res. 22, 267-281. https://doi.org/10.1081/rrs-120014601.





STAR***METHODS**

KEY RESOURCES TABLE

REAGENT or RESOURCE	SOURCE	IDENTIFIER
Antibodies		
DYKDDDDK Tag (D6W5B) Rabbit monoclonal antibody	Cell Signaling Technology	Cat#14793S; RRID: AB_2572291
Goat anti-rabbit IgG, polyclonal antibody (HRP conjugate)	Enzo Life Sciences	Cat#ADI-SAB-300-J; RRID: AB_11179983
Bacterial and virus strains		
TOP10 Escherichia coli strain	Invitrogen	Cat#C404003
DH10Bac Escherichia coli strain	Gibco	Cat#10361012
Chemicals, peptides, and recombinant proteins		
ESF921 incest cell culture medium	Expression system	Cat#96-001-20
Cellfectin™ II Reagent	Gibco	Cat#10352100
n-Dodecyl-β-D-Maltopyranoside	Anatrace	Cat#D310A
Cholesteryl hemisuccinate	Sigma-Aldrich	Cat#C6512
Glyco-disogenin	Anatrace	Cat#GDN101
Sodium cholate	Anatrace	Cat#S1010S
Leupeptin	Goldbio	Cat#L-010-5
Benzamidine	Sigma-Aldrich	Cat#B6506
Phenylmethylsulfonyl fluoride	Sigma-Aldrich	Cat#11359061001
Tris(2-carboxyethyl)phosphine hydrochloride	Goldbio	Cat#TCEP1
Guanosine 5'-diphosphate	Sigma-Aldrich	Cat#G7127
Apyrase	NEB	Cat#M0398L
Dulbecco's Modified Eagle Medium (DMEM)	Cytiva	Cat#SH30243.01
Fetal Bovine Serum	GW vitek	Cat#US-FBS-500
Antibiotic-Antimycotic	Gibco	Cat#15240-062
Lipofectamine 2000	Invitrogen	Cat#11668019
Coelenterazine h	Nanolight Technology	Cat#301
4% Paraformaldehyde	Tech&Innovation	Cat#BPP-9004
BSA	Bovogen Biologicals	Cat#BSAS 0.1
1-Step™ TMB-Blotting Substrate Solution	Thermofisher Scientific	Cat#34018
Janus Green B	Tokyo Chemical Industry	Cat#J0002
Cal-520	AAT Bioquest	Cat#21131
Neuropeptide Y	GL Biochem (custom peptide synthesis)	N/A
Neuropeptide Y(3–36)	GL Biochem (custom peptide synthesis)	N/A
Neuropeptide Y(18–36)	GL Biochem (custom peptide synthesis)	N/A
Peptide YY	GL Biochem (custom peptide synthesis)	N/A
Peptide YY(3–36)	GL Biochem (custom peptide synthesis)	N/A
Peptide YY(3–36)	APExBio	Cat#A1115
Critical commercial assays		
MG Plasmid DNA Mini Kit	MGmed	Cat#MK00020
NucleoBond Xtra Midi Plus kit	Macherey-Nagel	Cat#MN740412
Ni-NTA agarose	Qiagen	Cat#30230
HiTrap Q	Cytiva	Cat#17115301
Superdex 200 10/300 GL	Cytiva	Cat#28990945

(Continued on next page)

Article



Continued		
REAGENT or RESOURCE	SOURCE	IDENTIFIER
Deposited data		
Coordinates of NPY-Y ₂ R-G _i -scFv16 complex	This paper	PDB: 7YOO
Cryo EM map of NPY-Y ₂ R-G _i -scFv16 complex	This paper	EMDB: EMD-33985
Coordinates of PYY(3–36)–Y ₂ R–G _i –scFv16 complex	This paper	PDB: 7YON
Cryo EM map of PYY(3–36)–Y ₂ R–G _i – scFv16 complex	This paper	EMDB: EMD-33984
Experimental models: Cell lines		
Human Embryonic Kidney HEK293T	ATCC	Cat#CRL-3216
Spodoptera frugiperda Sf9	Expression systems	Cat#94-001F
Trichuplusia ni Hi5	Expression systems	Cat#94-002F
Recombinant DNA		
pFastBac-FLAG-BRIL-Y ₂ R-GFP-His-R1D4	This paper	N/A
pFastBac-Gα _i	This paper	N/A
pFastDual-His-Gβ, Gγ	This paper	N/A
pFastBac-scFv16-His	This paper	N/A
pcDNA3.1-FLAG-Y₁R	This paper	N/A
pcDNA3.1-FLAG-Y₂R (for wild-type receptor and point mutants)	This paper	N/A
pcDNA3.1-Gα _i	This paper	N/A
pcDNA3.1-Gβ	This paper	N/A
pcDNA3.1-Gγ	This paper	N/A
pcDNA3.1-FLAG-Y₁R-eYFP	This paper	N/A
pcDNA3.1-FLAG-Y ₂ R-eYFP (for wild-type receptor and point mutants)	This paper	N/A
pcDNA3.1-Gα _i -Rluc8	This paper	N/A
pcDNA3.1-Rluc8-β-arrestin 2	This paper	N/A
Software and algorithms		
Prism 9.3.0	GraphPad	https://www.graphpad.com/scientific- software/prism/
Cryosparc v.3.2	Punjani et al., 2017 ⁴⁴	https://cryosparc.com/
UCSF ChimeraX v1.1	Pettersen et al., 2021 ⁴⁵	https://www.cgl.ucsf.edu/chimerax/
Phenix v1.19.2–4158	Liebschner et al., 2019 ⁴⁶	https://phenix-online.org/
Molprobity	Williams et al., 2018 ⁴⁷	http://molprobity.biochem.duke.edu/
EMRinger	Barad et al., 2015 ⁴⁸	https://fraserlab.com/2015/02/18/ EMringer/
Pymol v2.5.0	Schrödinger	https://pymol.org/2/
Microcal PEAQ-ITC Analysis	Malvern Panalytical	https://www.malvernpanalytical.com/
Coot v.0.9.6	Emsley et al., 2010 ⁴⁹	https://www2.mrc-lmb.cam.ac.uk/ personal/pemsley/coot/
GROMACS 2018.6	Van Der Spoel et al., 2005 ⁵⁰	https://gromacs.org
VMD 1.9.4	Humphrey et al., 1996 ⁵¹	http://www.ks.uiuc.edu/Research/vmd
CHARMM-GUI	Jo et al., 2008 ⁵²	https://www.charmm-gui.org/
Alpha-Fold-Multimer	Evans et al., 2022 ⁵³	https://github.com/deepmind/alphafold/
GalaxyRefineComplex	Heo et al., 2016 ⁵⁴	https://galaxy.seoklab.org/refinecomplex
Galaxy7TM	Lee and Seok, 2016 ⁵⁵	http://galaxy.seoklab.org/7TM





RESOURCE AVAILABILITY

Lead contact

Further information and requests for resources and reagents should be directed to and will be fulfilled by the lead contact, Hee-Jung Choi (choihj@snu.ac.kr).

Materials availability

All unique/stable reagents generated in this study are available from the lead contact with a completed materials transfer agreement.

Data and code availability

- The PYY(3-36)-Y₂R-G_i-scFv16 and NPY-Y₂R-G_i-scFv16 structures were deposited in the PDB under the accession codes 7YON and 7YOO, and the electron density maps in the Electron Microscopy Data Bank under the accession codes EMD-33984 and 33985, respectively.
- This paper does not report original code.
- Any additional information required to reanalyze the data reported in this paper is available from the lead contact upon request.

EXPERIMENTAL MODEL AND SUBJECT DETAILS

Human Y₂R was expressed in Spodoptera frugiperda (Sf9) cells infected with recombinant baculovirus (pFastBac, Invitrogen). Heterotrimeric G_I and scFv16 were expressed in Trichoplusia ni (Hi5) cells infected with recombinant baculovirus (pFastBac, Invitrogen). Sf9 cells and Hi5 cells were grown in ESF921 medium (Expression systems) at 27°C. HEK293T cells were grown in Dulbecco's Modified Eagle Medium (DMEM; Cytiva) supplemented with 10% fetal bovine serum (GW vitek) and Antibiotic-Antimycotic (Gibco) at 37°C in an atmosphere containing 5% CO₂. HEK293T cells were acquired from (American Type Culture Collection, ATCC).

METHOD DETAILS

Expression and purification of Y2R

The full-length human Y₂R was modified to contain affinity tags (an N-terminal FLAG tag and a C-terminal 8xHis tag), stabilizing mutations (H149^{3.51}Y and S280^{6.47}C), and the stabilizing factor BRIL at the N-terminus to enhance receptor expression.²⁵ Modified Y₂R was cloned into a pFastBac vector with primers provided in Table S3 and the receptor was expressed in Sf9 cells using a Bac-to-Bac system (Invitrogen).⁵⁶ Cells were harvested 48 h after infection and were lysed with hypotonic buffer (20 mM HEPES (pH 7.5), 1 mM EDTA, protease inhibitors). Membrane fractions were collected by centrifugation (18,000 rpm, 20 min; 4°C) and were further solubilized in solubilization buffer (20 mM HEPES (pH 7.5), 150 mM NaCl, 1% n-dodecyl-β-D-maltopyranoside (DDM), 0.1% cholesteryl hemisuccinate (CHS), protease inhibitors) and purified using a Ni-NTA column. After column washing with high salt buffer (20 mM HEPES (pH 7.5), 0.5 M NaCl, 20 mM imidazole, 0.05% DDM, 0.005% CHS) and low salt buffer (20 mM HEPES (pH 7.5), 150 mM NaCl, 30 mM imidazole, 0.05% DDM, 0.005% CHS), bound receptor was eluted with low salt buffer containing 300 mM imidazole. For structural studies, the eluted receptor was further purified using a Superdex 200 10/300 size exclusion column (Cytiva) pre-equilibrated with 20 mM HEPES (pH 7.5), 150 mM NaCl, 0.03% DDM, and 0.003% CHS. Fractions containing BRIL-Y₂R-GFP were pooled, concentrated, and used directly to prepare the ligand-Y₂R-G_i complex. For ITC experiments, BRIL and GFP were cleaved by treatment with a HRV3C protease at 4°C overnight. Cleaved Y₂R was further purified using a Superdex 200 10/300 size exclusion column (Cytiva) pre-equilibrated with 20 mM HEPES (pH 7.5), 150 mM NaCl, 0.03% DDM, and 0.003% CHS. A peak fraction containing Y₂R was used for ITC experiments without any further concentration.

Expression and purification of heterotrimeric Gi

To purify the heterotrimeric G_i , human $G\alpha_{i1}$, $6xHis-G\beta_1$, and $G\gamma_2$ were co-expressed in Hi5 insect cells. Cells were harvested 48 h after infection and lysed with lysis buffer (20 mM Tris-HCI (pH 8.0), protease inhibitors). After centrifugation (18,000 rpm, 20 min; 4°C), G protein was solubilized with solubilization buffer (20 mM Tris-HCl (pH 8.0), 100 mM NaCl, 2 mM MgCl₂, 50 μM guanosine 5'-diphosphate (GDP), 1% sodium cholate, 0.1 mM Tris(2-carboxyethyl)phosphine hydrochloride (TCEP), protease inhibitors). Insoluble debris were removed by centrifugation and the supernatant was loaded onto a Ni-NTA column. During column washing, sodium cholate was gradually exchanged to DDM, and the bound protein was eluted with 20 mM Tris-HCl (pH 8.0), 100 mM NaCl, 1 mM MgCl₂, 10 μ M GDP, 0.03% DDM, 0.1 mM TCEP, and 300 mM imidazole. Eluted heterotrimeric Gi was further purified using a Hitrap Q column (Cytiva) pre-equilibrated with 20 mM Tris-HCl (pH 8.0), 1 mM MgCl₂, 10 μM GDP, and 0.03% DDM. Fractions containing G_i were pooled, concentrated, flash frozen in liquid nitrogen, and stored at -80°C until use.

Expression and purification of scFv16

Single-chain variable fragment (scFv16), which is a G_i-stabilizing antibody, was purified as previously described with slight modifications.⁵⁷ Briefly, scFv16 with a C-terminal 8xHis tag was expressed in Hi5 cells. After cell harvesting, the supernatant containing the secreted scFv16 was incubated with Ni-NTA resin for 2 h at 4°C. The resin was washed with washing buffer (20 mM Tris-HCl

Article



(pH 7.5), 150 mM NaCl, and 30 mM imidazole), and the bound protein was eluted with washing buffer supplemented with 300 mM imidazole. Eluted protein was further purified by size exclusion chromatography on a Superdex 200 10/300 gel filtration column (Cytiva) pre-equilibrated with 20 mM HEPES (pH 7.0) and 150 mM NaCl. Purified scFv16 was concentrated, flashed frozen in liquid nitrogen, and stored at -80° C until use.

Y₂R complex purification

To prepare the NPY- Y_2R - G_i -scFv16 and PYY(3-36)- Y_2R - G_i -scFv16 complexes, synthesized ligands and each purified protein (BRIL- Y_2R - G_i -scFv16) were mixed in a 2:1:1.2:1.5 M ratio (ligand: Y_2R : G_i :scFv16) and incubated at 4°C overnight. Each protein mixture was loaded onto an anti-GFP nanobody column to remove excess G_i and scFv16. After on-column detergent exchange from DDM to glyco-diosgenin (GDN), the samples were treated with a HRV3C protease to obtain each ligand- Y_2R - G_i -scFv16 complex. A final size exclusion chromatography purification was performed using a buffer consisting of 20 mM HEPES (pH 7.5), 150 mM NaCl, 0.01% GDN, 0.001% CHS, and 2 μ M ligand. Each purified complex was concentrated to 8–10 mg ml⁻¹ and used for grid preparation.

Cryo-EM grid preparation and data collection

For each Y_2R complex, a $4.5~\mu L$ aliquot was applied onto a glow discharged holey carbon grid (Quantifoil R1.2/1.3, 200 mesh). The grids were blotted for 3.5~s under 100% humidity at $4^{\circ}C$ and vitrified by plunging into liquid ethane using a Vitrobot Mark IV (Thermo Fisher Scientific, SNU CMCI). Cryo-EM data collection for both complexes was performed using a 300 kV Krios G4 (Thermo Fisher Scientific) equipped with K3 direct electron detector and Gatan GIF quantum energy filter at the Institute for Basic Science (IBS, Korea). For the NPY-bound complex, movies were recorded in counting mode at a pixel size of 0.841~Å and a defocus range of $-1~\mu$ m to $-2.25~\mu$ m. A total of 9,228 movies were collected, each comprising 60 frames, with a total dose of 66 electrons per Å^2 . For the PYY(3–36)-bound complex, movies were recorded in counting mode at a pixel size of 0.849~Å and a defocus range of $-0.75~\mu$ m to $-2.0~\mu$ m. A total of 13,559 movies were collected, each comprising 57 frames, with a total dose of 60.5 electrons per Å^2 .

Cryo-EM data processing

For the NPY-Y₂R-G_i-scFv16 and PYY(3-36)-Y₂R-G_i-scFv16 complexes, collected movies were subjected to patch motion correction and patch contrast transfer function (CTF) estimation implemented in cryoSPARC v.3.2 ⁴⁶. Damaged micrographs and micrographs with a CTF fit lower than 5 Å were discarded after this process. Particles selection was performed with a blob picker using partial fraction of the movies. These particles were further processed for 2D Classification and fine 2D templates were used for template picker. For NPY-Y₂R-G_i-scFv16, initial template picking resulted in 9,842,630 particles from 8752 movies. These particles were further subjected to four rounds of 2D classification, three rounds of heterogeneous refinement, and a local motion correction leaving 500,366 particles for final reconstruction. These particles were used for non-uniform refinement yielding a 3.11 Å resolution map. To further enhance the quality of the extracellular region, local refinement was conducted by masking the TM region, resulting in a 3.39 Å resolution map. To combine the maps, $G\alpha_i\beta\gamma$ -scFv16 was masked and used for local refinement yielding a 3.04 Å resolution map. Local resolution was determined using local resolution estimation implemented in cryoSPARC v.3.2. These two maps were merged using vop-maximum in UCSF ChimeraX v.1.1 ⁴⁷ and used for further structure refinement. Angular distribution of the particles was visualized using "star2build" script implemented in pyem.⁵⁸

For the PYY(3–36)–Y₂R–G_i–scFv16 complex, the initial template picking resulted in 12,262,301 particles from 13,559 movies. These particles were further subjected to five rounds of 2D classification and two rounds of heterogeneous refinement, leaving 359,459 particles for final reconstruction. These particles were used for non-uniform refinement yielding a 2.95 Å resolution map. To further enhance the quality of the extracellular region, local refinement was conducted by masking the TM region resulting in a 3.15 Å resolution map. To combine the maps, G_i–scFv16 was masked and used for local refinement yielding a 2.89 Å resolution map. Local resolution was determined using local resolution estimation implemented in cryoSPARC v.3.2. These two maps were merged using vop-maximum in UCSF ChimeraX v.1.1 ⁴⁵ and used for further structure refinement. The angular distribution of the particles was visualized using "star2build" script implemented in pyem.⁵⁸

Model building and refinement

Initial models were assembled with the inactive Y₂R structure (PDB: 7DDZ), and NPY, G_i, scFv16 structure (PDB: 7VGX) with a rigid-body and simulated annealing in Phenix v.1.19.2–4158. Because the inactive Y₂R structure was lacking the N-terminus and the ICL3, poly-A chain was added to the structure and each residue was fitted based on the map. For PYY(3–36), NPY was used as a base model and the different residues were mutated into the amino acids of PYY. This model was then subjected to multiple rounds of manual rebuilding with COOT⁴⁹ and real-space refinement implemented in Phenix v.1.19.2–4158. The geometry of the final structure was evaluated using MolProbity⁴⁷ and EMRinger. Figures were prepared using UCSF ChimeraX v1.1 and PyMol v2.5.0. Refinement statistics are summarized in Table 1.

Molecular dynamics simulation

To generate the initial model for MD simulations, the missing residues were added to the structural model of NPY-Y₂R-G_i complex. The α -helical domain of G α _i was added by aligning the previously reported structure, ⁵⁹ and the missing residues of NPY (9–15) were





built based on the unsharpened map of NPY-Y₂R at a lower threshold. The missing residues at the N-terminus of Y_2 R (2-39) were built randomly. This study used the CHARMM36(m) force field for proteins and lipids. 60-62 The TIP3P water model was utilized along with 0.15 M NaCl solution. All simulations were performed using the inputs generated by CHARMM-GUI and GROMACS 2018.6 for both equilibration and production with the LINCS algorithm. 50,63-66 Three independent MD simulations were performed for each system to obtain better sampling and check the convergence. Long-range electrostatic interactions were calculated using the particle-mesh Ewald method with a mesh size of \sim 1 Å and the van der Waals interactions were smoothly switched off over 10–12 Å by a force-based switching function. ^{67,68} For pressure coupling (1 bar), the semi-isotropic Parrinello-Rahman method with a τ_p of 5 ps and compressibility of 4.5×10^{-5} bar⁻¹ was used.⁶⁹ To maintain the temperature, the Nosé-Hoover thermostat was used with $\tau_1 = 1$ ps. The constant particle number, volume, and temperature dynamics were first applied with a 1-fs time step for 250 ps during the equilibration run. Subsequently, the constant particle number, pressure, and temperature ensemble was applied with a 1-fs time step (for 2 ns) and with a 2-fs time step (for 18 ns). During the equilibration, positional and dihedral restraint potentials were applied, and their force constants were gradually reduced. The production run was performed with a 4-fs time step using the hydrogen mass repartitioning technique without any restraint potential. 70 Each system ran approximately 25 ns/day with 512 CPU cores on NURION in the Korea Institute of Science and Technology Information.

Isothermal titration calorimetry

Isothermal titration calorimetry was performed using a MicroCal Auto-iTC200 (Malvern Panalytical) to assess the binding affinity between the peptide and the receptor. Freshly purified 10–20 μM of Y₂R and 150–300 μM PYY, NPY, and NPY(18–36). Each titration experiment was performed by injecting 1.5 μ L of peptides for 30 times at 120 s intervals and 25 $^{\circ}$ C. The basal heat signal was acquired by injecting each peptide to the size exclusion chromatography buffer. Data analysis was performed using the MicroCal PEAQ-ITC Analysis software.

BRET assay

For Y₁R/Y₂R-G protein BRET dose-response assay, HEK293T cells were plated in 6-well plates and co-transfected with Gα_i-Rluc8, Gβ, Gγ, and Y₁R/Y₂R-eYFP at a 1:2:2:5 ratio. All the oligonucleotides used in generation of Y₂R-eYFP constructs carrying T138^{3.40}I, H155^{ICL2}P and T266^{6.33}I mutation are provided in Table S3. For Y₁R/Y₂R-β-arrestin 2 BRET dose-response assay, HEK293T cells were co-transfected with Rluc8-β-arrestin 2 and Y₁R/Y₂R-eYFP at a 1:8 ratio. Rluc8 is inserted between L91 and K92 of human $G\alpha_{i}$, and at the N-terminus of human β -arrestin 2, respectively. EYFP is inserted at the C-terminus of Y_2R with three alanine linker. Forty-eight hours after transfection, the cells were detached with 1X PBS supplemented with 20 mM EDTA. The detached cells medium was exchanged into 1X HBSS supplemented with 10 mM HEPES (pH 7.5). Cells were treated with NPY/PYY/PYY(3-36) at the desired final concentration and plated into 96-well white plates. For Y₁R/Y₂R, β-arrestin 2 transfected cells were further incubated at 37°C for 10 min Rluc8 and eYFP signals were each measured at 480 and 540 nm for 30 min after 5 μM coelenterazine h (Nanolight Technology) was injected using Tristar² LB942 (Berthold Technologies). ΔBRET was calculated by subtracting the BRET ratio detected in vehicle-stimulated cells from the BRET ratio detected in NPY-treated cells. Data analysis and presentation was performed using GraphPad Prism 9.3.0.

ELISA-based surface expression assay

HEK293T cells were transfected with a pcDNA3.1 plasmid containing an N-terminal FLAG tag and various Y₂R mutants. All the oligonucleotides used in generation of Y₂R mutants are provided in Table S3. After 48 h, cells were fixed by treatment with 4% paraformaldehyde (Tech&Innovation) and washed with 1X PBS. Cells were incubated with a blocking solution consisting of 1X PBS and 5% BSA (Bovogen Biologicals) for 1 h. A rabbit anti-FLAG (Cell signaling Technology) and goat anti-rabbit HRP (Enzo Life Sciences) antibodies were added sequentially. 1-StepTM TMB-Blotting Substrate Solution (Thermofisher Scientific) was added to each well for detection, and 1 M HCl was added to stop the reaction. The absorbance was detected at 450 nm using a FlexStation 3 multi-mode microplate reader (Molecular Devices). Normalization was carried out by mitochondria staining. The remaining solution in each well was removed, and a 0.2% (w/v) Janus Green B (Tokyo Chemical Industry) solution was added. After 5 min of incubation, the excess stain was eliminated by extensive washing with distilled water. Stain was eluted with 0.5 M HCl, and the absorbance was measured at 595 nm. The normalized expression level of the receptor at the cell surface was calculated by the ratio of the absorbance at 450 and 595 nm (A₄₅₀/A₅₉₅). The graphs were plotted using GraphPad Prism 9.3.0.

Ca²⁺ signaling assay

HEK293T cells were seeded in 96-well black wall/clear bottom microplates (Greiner Bio-One). Cells were transfected with a plasmid containing Y_1R/Y_2R , $G\alpha_{\Delta 6 \text{qi/amyr}}$, $G\beta$, and $G\gamma$ in a 3:1:1:1 ratio. ⁷² After 48 h of incubation, cells were stained with 5 μ g/mL Cal-520 (AAT Bioquest) in assay buffer (HBSS, 0.1% BSA, 20 mM HEPES (pH 7.4)) for 2 h. The cells were then washed with assay buffer to remove excess dye. The intracellular Ca^{2+} influx was measured at Ex/Em = 490/525 nm for 130 s using the FlexStation 3 multi-mode microplate reader (Molecular Devices). NPY peptides diluted in assay buffer were transferred to each well at 30 s. Among the measured signals, the 0-30 s section was taken as the baseline and the relative fold of the 30-130 s section was calculated. EC₅₀ values were calculated by plotting log(concentration)-response curves using GraphPad Prism 9.3.0, by fitting an agonist response curve with a variant slope.

Article



Modeling of NPY-bound Y₅R

Y₅R in complex with the NPY peptide was initially modeled using Alpha-Fold-Multimer.⁵³ G protein was included during modeling to obtain the active form of Y₅R. The structural models were then refined using GalaxyRefineComplex⁵⁴ and a scoring function optimized for GPCR structure prediction.⁵⁵ The top scoring structure was used for comparison.

QUANTIFICATION AND STATISTICAL ANALYSIS

Cryo-EM data were processed using cryoSPARC v.3.2,44 UCSF ChimeraX v.1.1,45 and pyem.58 Cryo-EM structure statistics were analyzed using MolProbity⁴⁷ and EMRinger.⁴⁸ ITC data were analyzed using the MicroCal PEAQ-ITC Analysis software. Statistical details for ITC are provided in Figure S1 and its legend. ELISA, BRET, and Ca2+ signaling assay data were analyzed using GraphPad Prism 9.3.0. Statistical details for Ca2+ signaling assays and BRET experiments are provided in Figures 2, 3, 5, Tables S1 and S2, and their legends. For ELISA experiments, the statistical details are provided in Figure S2 and its legend.